

1 **BIPV/T facades – a new opportunity for Integrated Collector-** 2 **Storage Solar Water Heaters?**

3 ***Part 2: Physical realisation and laboratory testing***

4
5 Adrian Pugsley^(a) (a.pugsley@ulster.ac.uk, +44(0)28 90366264 (corresponding author)
6 Aggelos Zacharopoulos^(a) (a.zacharopoulos@ulster.ac.uk) +44(0)28 90368227
7 Jayanta Deb Mondol^(a) (jd.mondol@ulster.ac.uk) +44(0)28 90368037
8 Mervyn Smyth^(a, b) (m.smyth1@ulster.ac.uk) +44(0)28 90368119

9 (a) Centre for Sustainable Technologies (www.cst.ulster.ac.uk), School of the Built
10 Environment, Ulster University, Newtownabbey, BT37 0QB, Northern Ireland, UK

11 (b) SolaForm Ltd (www.solaform.com) c/o Ulster University, Newtownabbey, BT37 0QB,
12 Northern Ireland, UK
13

14 **Keywords**

15 Integrated Collector-Storage Solar Water Heaters (ICSSWH); Photovoltaic-Thermal
16 (PV/T); thermal diode; building facade; solar collector; heat removal factor
17

18 **Highlights**

- Two-part study proposing an alternative approach to realising BIPV/T facades
- Part 1 reviews theory & potential, Part 2 describes prototype realisation & testing
- Integrated Collector-Storage Solar Water Heater (ICSSWH) element reduces overheating
- Planar Liquid-Vapour Thermal Diode (PLVTD) element reduces overnight heat losses
- Experimental results offer BIPV-PLVTD-ICSSWH benchmarks & validate theoretical model

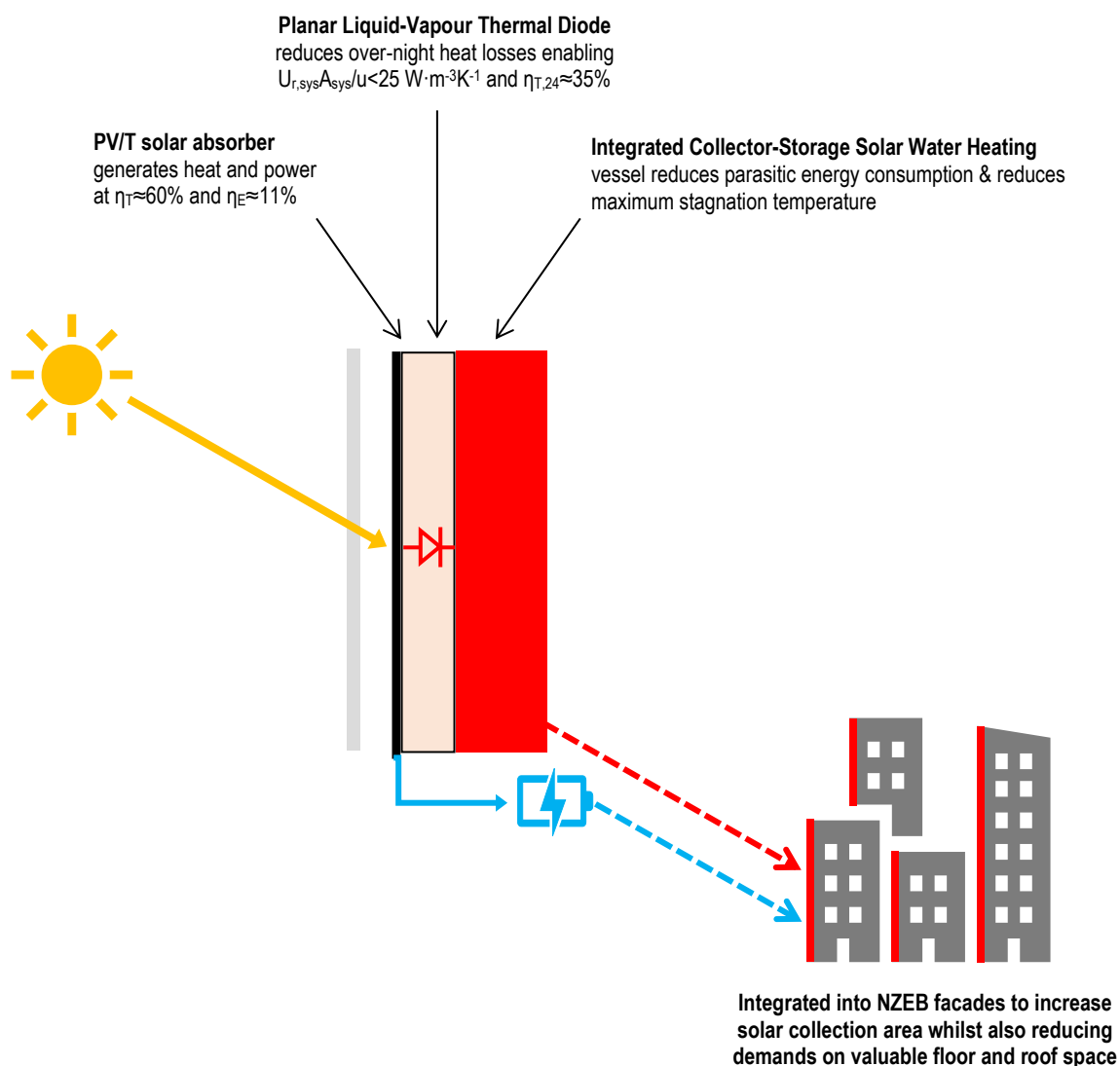
19

20 **Abstract**

21 Building Integrated Photovoltaic Thermal (BIPV/T) systems which generate electricity
22 and heat simultaneously are promising solutions for Net Zero Energy Buildings (NZEB).
23 Despite BIPV/T offering clear energetic and space saving advantages compared to
24 separate PV and solar thermal, overheating problems occur when no thermal demand
25 exists, resulting in reduced yields, stagnation damage, and excessive fluid flow
26 pressures. This two-part study examines an alternative approach combining BIPV,
27 Planar Liquid-Vapour Thermal Diodes (PLVTD) and Integrated Collector-Storage Solar
28 Water Heaters (ICSSWH) to achieve BIPV/T functionality and retain heat overnight to
29 minimise parasitic demands and reduce overheating. The introductory paper (Part 1
30 of 2) established novelty and rationale for BIPV-PLVTD-ICSSWH concepts, reviewed

31 state-of-the-art and performance benchmarks, and used theoretical modelling to
32 predict behaviour from key design and operational parameters. This paper (Part 2 of
33 2) describes prototype realisation and multi-day solar simulator laboratory thermal and
34 photovoltaic testing for covered and uncovered variants exposed to different irradiance
35 levels. Measured solar thermal efficiencies with and without transparent covers were
36 $\eta_{T,col} = 60\%$ and 58% respectively under zero heat loss conditions whilst overnight
37 heat loss coefficients were $U_{r,sys}A_{sys}/u = 23.0$ and $25.4 \text{ W}\cdot\text{m}^{-3}\text{K}^{-1}$ respectively, showing
38 good agreement with theoretical predictions. Photovoltaic performance reduced with
39 increasing absorber temperature as expected, although maximum power point
40 efficiencies ($\eta_{E,mpp} = 11.4\%$ at $T_1 \approx 25^\circ\text{C}$ and 5.6% at $T_1 \approx 89^\circ\text{C}$, without cover) were
41 lower than expected owing to partial delamination and PV cell damage. The work
42 demonstrates practical operation of a vertical BIPV-PLVTD-ICSSWH, identifies key
43 areas for design development, and highlights benefits of application in NZEB facades.

44 **Graphical abstract**



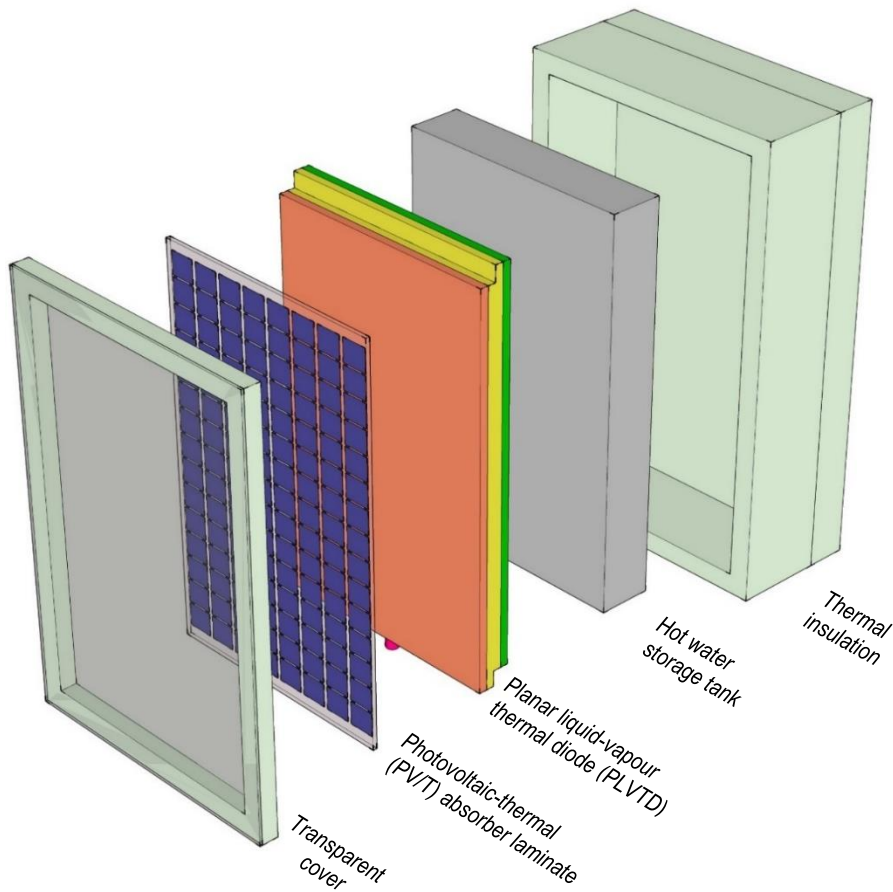
47 **1 Introduction**

48 Net Zero Energy Buildings (NZEB) and Near Zero Energy Buildings (nZEB) are
49 increasingly being designed with Building Integrated Photovoltaics (BIPV) to generate
50 electricity and Building Integrated Solar Thermal Systems (BISTS) to supply domestic
51 hot water and contribute towards space heating demands (COST, 2015; Good, 2015).
52 Mismatches between energy demands and solar availability (instantaneously, diurnally
53 and over inter-seasonal timescales) mean that thermal energy storage is an essential
54 part of most BISTS and is crucial for achievement of a high solar fraction (Affolter et
55 al., 2006; Drosou et al., 2014). Electrical energy storage is likewise crucial for high
56 solar fraction BIPV systems (Kats and Seal, 2012; Sorgato et al., 2018; Belussi et al.,
57 2019). Building Integrated Photovoltaic-Thermal (BIPV/T) façade systems combine
58 solar electricity and thermal energy (hot air and/or water) generation into vertical
59 elements of building envelopes to make efficient use of all available insulated surfaces
60 (Zondag, 2008; Yang & Athienitis, 2016). This is important for NZEBs where there is
61 a high ratio of energy demand to envelope surface area, and in particular to the case
62 of tall buildings where roof space for solar collectors is inherently limited. The most
63 common realisation of water-heating PV/T collectors is to bond a conventional PV
64 module to the absorber of a conventional sheet-and-tube flat solar water heater
65 (Dupeyrat et al., 2011; Calise et al., 2016) or other planar heat removal device
66 (Kazemian et al., 2018; Fayaz et al., 2019). Despite offering clear energetic
67 advantages when suitable thermal demands exist, PV/T collectors suffer similar
68 stagnation and overheating problems as closed-back BIPV systems (ie reduced
69 electrical yields and eventual delamination damage) and conventional solar flat plate
70 solar water heaters (ie over-pressurisation, denaturing of heat transfer fluids, damage
71 to selective coatings, melting of polymeric components) when no thermal demands
72 exist (Dupeyrat et al., 2011; Hasanuzzaman et al., 2016; Lazzarin and Noro, 2019).
73 Stagnation overheating can be avoided by ensuring continuous fluid flows on hot sunny
74 days but the corresponding parasitic energy requirements (eg for pumps and/or heat
75 rejection fans) would have potential to far exceed the corresponding modest gains in
76 electrical yields and the ancillary equipment needed (large thermal stores and/or heat
77 rejectors) occupies valuable floor space.

78 Integrated Collector-Storage Solar Water Heaters (ICSSWH) are an alternative to
79 conventional flat plate or evacuated tube collector solar water heating systems. Whilst

80 ICSSWH systems suffer significant overnight heat losses (eg unavailability of stored
81 heat for morning bathing etc) they offer a number of advantages in respect of cost,
82 space, and inherent passive protection from overheating. Recent studies by Pugsley et
83 al. (2016, 2017, 2019, 2020) proposed the use of Planar Liquid-Vapour Thermal Diodes
84 (PLVTD) to reduce problems of overnight heat loss in flat-form ICSSWH collectors.
85 Studies by Krauter (2004) and Ziapour et al. (2014) examined the performance
86 (respectively through experimental and simulation work) of novel PV-ICSSWH devices
87 and identified a dearth of published work on similar concepts. Development of the
88 novel BIPV-PLVTD-ICSSWH approach proposed in this two-part study has the potential
89 to overcome key problems associated with the individual technologies (namely, BIPV/T
90 overheating during stagnation, and ICSSWH overnight heat losses) and to realise new
91 synergies. An exploded diagram illustrating the component parts of a BIPV-PLVTD-
92 ICSSWH collector is shown in Figure 1. The fundamental principles of PV/T, ICSSWH
93 and PLVTD concepts underpinning this study were reviewed in our introductory paper
94 (Part 1 of 2) which also established state-of-the-art performance benchmarks and
95 examined the expected energetic behaviour using a theoretical heat transfer model.
96 The present paper (Part 2 of 2) concludes the study on this novel approach to BIPV/T
97 by describing the realisation of a BIPV-PLVTD-ICSSWH prototype and presenting
98 results of multi-day solar simulator laboratory tests for covered and uncovered variants
99 exposed to different irradiance levels. This paper presents the measured temperatures,
100 solar thermal collection, photovoltaic generation, and overnight heat retention
101 efficiencies to establish performance benchmarks for the first ever BIPV-PLVTD-
102 ICSSWH prototype, and compares these against theoretical modelling predictions in
103 order to validate the model and identify key aspects of the design which can be
104 improved. The key benefits and challenges associated with practical implementation of
105 BIPV-PLVTD-ICSSWH concepts to support realisation of NZEBs as part of global
106 decarbonisation efforts to tackle the climate crisis is also reviewed, with specific focus
107 on building façade and heat pump system integration.

108



109
 110 *Figure 1: Key components of the BIPV-PLVTD-ICSSWH concept*

111

112 **2 Operating principles and performance benchmarks**

113 The fundamental physical arrangement of the BIPV-PLVTD-ICSSWH device proposed
 114 in Figure 1 can be represented by the lumped parameter model shown in Figure 2. The
 115 model describes how the input solar irradiance (G) passes through transparent cover
 116 layers (optical transmissivity τ) before being absorbed by the PV cells (solar
 117 absorptivity α and temperature T_0) which convert the incident solar flux into thermal
 118 energy and electrical energy. The thermal power is either lost (q_{0a}) to the ambient
 119 environment (at temperature T_a) or transferred (q_{03}) through the thermal diode via the
 120 evaporator (at temperature T_1) and condenser (at temperature T_2) to heat the water
 121 storage tank (at temperature T_3) where it becomes available for delivery to thermal
 122 loads (q_T). Some of the solar heat gained by the tank is lost through the insulated tank
 123 sidewalls and back plate (q_{3ia}). Thermal diode heat losses (q_{4ia}) from the insulated
 124 PLVTD sidewalls (at temperature T_4) are neglected as these are small by comparison.
 125 Absorber heat losses (q_{0a}) pass through the absorber laminate (from the cells at
 126 temperature T_0 to the front surface at T_5) and airgap to the transparent cover (at

127 temperature T_6) and eventually to the ambient. The amount of electrical power
128 produced by the PV cell array ($q_E = I_{PV} \cdot V_P$) is dependent upon the irradiance; the pump
129 and load electrical resistances; and the PV cell array electrical characteristics, which
130 are themselves dependent upon the PV cell material properties and temperature. Some
131 of the electrical power generated by the PV is delivered to a small pump (q_P) which
132 distributes a working fluid film to wet the PLVTD evaporator and the remainder (q_{load})
133 is available to serve applied electrical loads. Further details of the theoretical model
134 together with corresponding mathematical expressions and scenario simulations are
135 presented in a separate paper (Part 1 of 2) which serves as the introduction to this
136 two-part study.

137 Thermal power gained by an ICSSWH during solar collection periods is usually
138 determined using either quasi steady-state or whole-day testing based upon the rate
139 of temperature rise of the stored thermal mass ($q_T = M \cdot c_p \cdot \Delta T_3 / t_{col}$) where q_T is the heat
140 gain, $M \cdot c_p$ is the mass and specific heat capacity product of the thermal store, and ΔT_3
141 is the rise in thermal store temperature during a collection period of duration t_{col} . Loss
142 of stored heat overnight is likewise determined in a similar manner with reference to
143 the heat retention period duration t_{ret} . Equations 1 to 3 define the solar thermal
144 collection efficiency ($\eta_{T,col}$), heat retention efficiency ($\eta_{T,ret}$), and heat loss coefficient
145 ($U_{r,sys} A_{sys}$). Collection efficiencies are evaluated with reference to total insolation (H)
146 which is the product of the irradiance (G) incident on the collector aperture (area A_1)
147 during the collection period. Retention efficiencies are evaluated with reference to the
148 amount of heat contained within the thermal store at the start of the retention period
149 (assumed to commence at the end of the preceding collection period) and are
150 normalised in relation to ambient temperatures at the end of the collection period
151 ($T_{a[t_{col}]}$) and averaged throughout the retention period ($\bar{T}_{a[t_{ret}]}$). Collection performance
152 is influenced by the solar thermal condition (Equation 4) such that the highest
153 efficiencies occur when the stored water temperature is close to the ambient
154 temperature (zero heat loss when $N=0$ because $T_3=T_a$) and efficiency reduces with
155 increasing ΔT_{3a} , especially when the irradiance is low. The introductory paper of this
156 study (Part 1 of 2) established $\eta_{T,col} \approx 60\%$ at $N \approx 0.035 \text{ m}^2 \text{K} \cdot \text{W}^{-1}$ as a state-of-the-art
157 benchmark for ICSSWH collection efficiency and also established benchmark specific
158 heat loss coefficients of $U_{r,sys} A_{sys} / A_1 \approx 1 \text{ W} \cdot \text{m}^{-2} \text{K}^{-1}$ and $U_{r,sys} A_{sys} / u \approx 10 \text{ W} \cdot \text{m}^{-3} \cdot \text{K}^{-1}$ at
159 $\Delta T_{3a} \approx 25^\circ \text{C}$, where u is the water storage tank volume. Heat could feasibly be drawn

160 to serve thermal load demands at any time of day (eg morning or evening bathing,
 161 space heating at night, etc) hence Equation 5 describes the diurnal thermal efficiency
 162 ($\eta_{T,24}$) which is a composite of the collection and retention efficiencies. Provided that
 163 t_{col} and t_{ret} cover a contiguous 24 hour period then $\eta_{T,24}=1$ describes the hypothetical
 164 case where all available solar energy is collected and then retained without loss,
 165 whereas $\eta_{T,24}=0$ would occur if no heat was collected or all collected heat was lost.

166 Photovoltaic cells and modules are commonly characterized with reference to Standard
 167 Test Conditions (STC at $G=1000 \text{ W/m}^2$ irradiance with spectrum AM1.5 and $T_0=25^\circ\text{C}$
 168 cell temperature) using performance metrics derived from current-voltage curves.
 169 Performance of PV/T collectors commonly deviates significantly from that occurring
 170 under STC because cells are operated at elevated temperatures in order to deliver
 171 useful heat. The cell temperature (T_0) is determined by the absorber temperature (T_1)
 172 which in turn is determined by a combination of ambient temperature (T_a) and fluid
 173 delivery temperature (T_3). The inclusion of transparent covers over the absorber
 174 reduces the influence of T_a to enable high T_3 and/or operation in cold and windy
 175 climates but unfortunately covers also introduce optical losses which reduce the level
 176 of irradiance incident on the PV cells. Key performance metrics for PV elements
 177 (defined in Equations 6 to 9) include short circuit current (I_{sc}), open circuit voltage
 178 (V_{oc}), electrical power delivered at the maximum power point ($q_{E,mp}$), fill factor (FF),
 179 voltage-temperature coefficient ($K_{V:T}$), current-temperature coefficient ($K_{I:T}$) and
 180 voltage-irradiance coefficient ($K_{V:G}$).

$$181 \quad \eta_{T,col} = \frac{\text{Energy in store at } t=t_{col}}{\text{Energy incident from } t=t_0 \text{ to } t=t_{col}} = \frac{M \cdot c_p (T_3[t=t_{col}] - T_3[t=t_0])}{H \cdot A_1} \quad \text{Equation 1}$$

$$182 \quad \eta_{T,ret} = \frac{\text{Retained energy in store at } t=t_{col}+t_{ret}}{\text{Energy in store at } t=t_{col}} = \frac{M \cdot c_p (T_3[t=t_{col}+t_{ret}] - \tilde{T}_a[t_{ret}])}{M \cdot c_p (T_3[t=t_{col}] - T_a[t=t_{col}])} \quad \text{Equation 2}$$

$$183 \quad U_{r,sys} A_{sys} = \frac{M \cdot c_p}{t_{ret}} \ln \left(\frac{1}{\eta_{T,ret}} \right) \quad \text{Equation 3}$$

$$184 \quad N = \frac{\tilde{T}_3 - \tilde{T}_a}{t_{col} \int_{t=0}^{t=t_{col}} G} \quad \text{Equation 4}$$

$$185 \quad \eta_{T,24} = \eta_{T,col} \cdot \eta_{T,ret} \quad \text{Equation 5}$$

186 $q_{E,mp} = I_{mp} \cdot V_{mp} = FF \cdot I_{sc} \cdot V_{oc}$ Equation 6

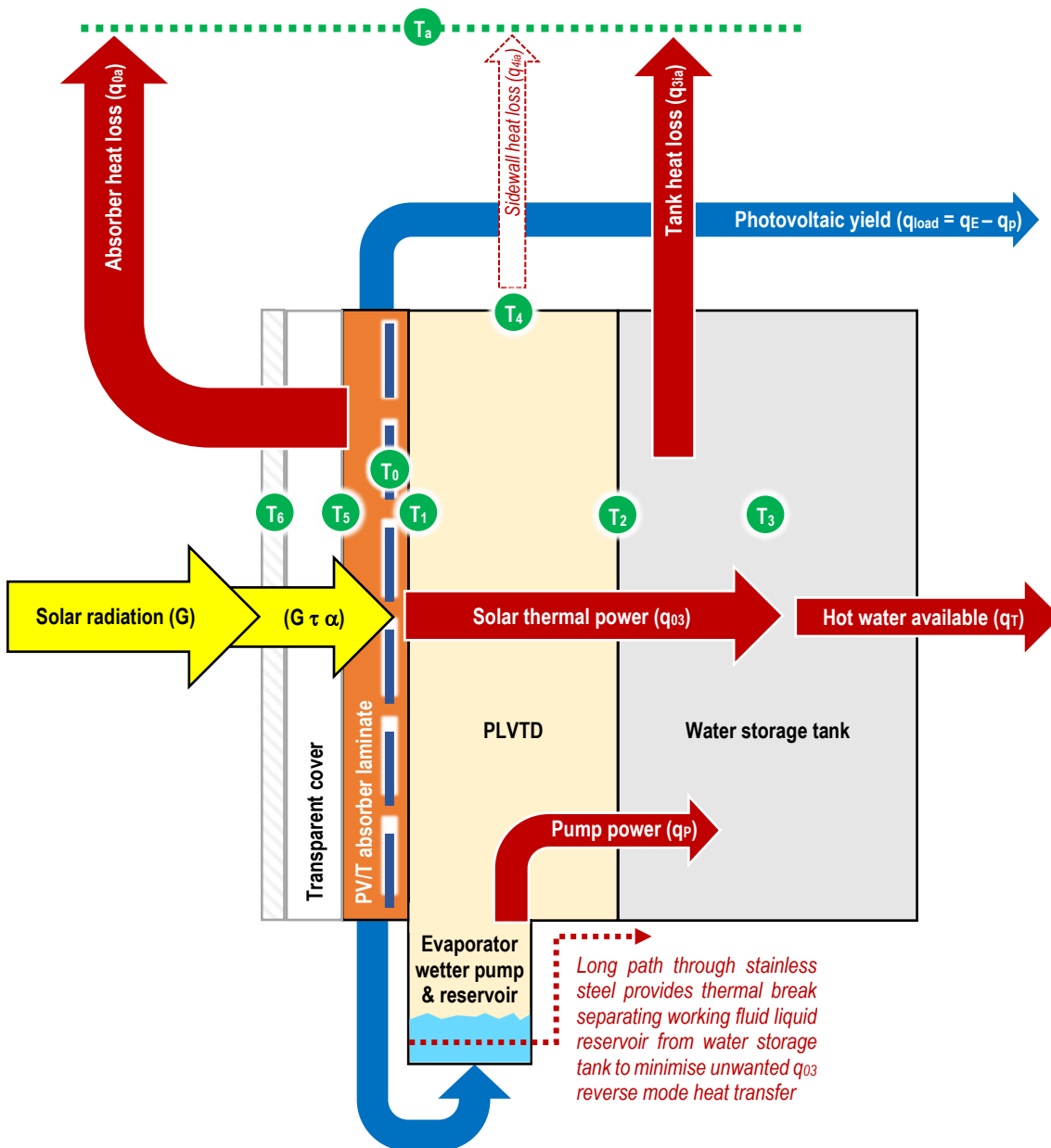
187 $K_{V:T} = \frac{V_{oc,T_0} - V_{oc,STC}}{V_{oc,STC} (T_0 - 25)}$ Equation 7

188 $K_{I:T} = \frac{I_{sc,T_0} - I_{sc,STC}}{I_{sc,STC} (T_0 - 25)}$ Equation 8

189 $K_{V:G} = \frac{V_{oc,G}}{V_{oc,STC}}$ Equation 9

190

191



192

193

G	Incident solar radiation flux	$G\tau\alpha$	Absorbed solar radiation
T_a	Ambient environmental temperature	q_{03}	Thermal power transferred from the absorber to the water storage tank through the thermal diode
T_0	Photovoltaic cell temperature	q_T	Net rate of heat gained by the stored water bulk
T_1	Temperature of absorber laminate substrate and PLVTD evaporator plate	q_{0a}	Heat loss from PV cells
T_2	Temperature of condenser plate and tank mantle	q_{3ia}	Heat loss from the back and sides of the water storage tank not covered by the thermal diode
T_3	Temperature of water bulk stored in the tank	q_{4ia}	Heat loss from PLVTD sidewalls
T_4	Thermal diode sidewall temperature	q_E	Electrical power yielded from PV
T_5	Absorber laminate surface temperature	q_P	Electrical power consumed by the evaporator wetter pump which is then all converted to heat
T_6	Transparent cover temperature	q_{load}	Electrical power delivered to load

194

Figure 2: Lumped parameter model of a BIPV-PLVTD-ICSSWH

195 **3 Experimental work**

196 **3.1 Design and realisation of a prototype**

197 The design of a laboratory prototype BIPV-PLVTD-ICSSWH collector was developed
198 with due consideration for constraints imposed by building and façade integration (see
199 Section 4). A prototype with $z=1400$ mm high by $y=700$ mm wide absorber and 100L
200 capacity water storage tank was fabricated, consisting of the key components
201 illustrated on Figure 1 with properties as detailed in Table 1:

- 202 1) Removable transparent acrylic cover set over a sealed air-filled cavity in order
203 to insulate against solar absorber heat losses.
- 204 2) Solar PV/T absorber formed of 120 quartered mc-si PV cell pieces (78x78mm)
205 covered by transparent acrylic plates bonded to the matt black painted PLVTD
206 evaporator plate using transparent silicone resin. The PV cell pieces were
207 arranged as 15 separate strings (each forming a row of 8 cell pieces, as shown
208 on Figure 3) and bonded to, and electrically isolated from, the stainless steel
209 substrate by 5 small pieces of 1mm thick self-adhesive polyurethane foam. The
210 PV cells were electrically interconnected in a series-parallel configuration on 5
211 buses (labelled A to E on Figure 3) to produce $V_{oc} \approx 24$ V and sufficient current
212 ($I_p \approx 0.5$ A) to drive the evaporator wetter pump.
- 213 3) Stainless steel PLVTD constructed of 0.9mm plates and sidewalls with 200
214 cylindrical tubular internal support struts. A novel cross-sectional shape was
215 developed to enable integration of the working fluid reservoir without causing a
216 liquid thermal bridge (see Figures 2&4). The evaporator wetting system
217 consisted of a small manifold-mount centrifugal pump fitted to the reservoir
218 base with a stainless steel pipe supplying fluid to a linear distribution nozzle at
219 the head of the evaporator plate to create a falling film. Refer to Pugsley (2017)
220 and Pugsley et al. (2020) for further details concerning PLVTD design attributes.
- 221 4) Flat profile open-top water storage tank formed of stainless steel sheet folded
222 into a 4-sided rectangular box shape, welded to the PLVTD condenser plate, and
223 insulated externally on all sides (including lid) with polystyrene foam.

224 Prototype fabrication commenced with the metalwork fabrication (see Pugsley, 2017;
225 Pugsley et al., 2020 for more details) according to the arrangement shown on Figure 4.
226 After repairing minor envelope vacuum leaks at welded joints, the PLVTD enclosure
227 was evacuated to 0.01 kPa, which removed non-condensable gases and enabled
228 injection of 0.9kg working fluid through an arrangement of valves. The prototype was

229 then mounted on a frame before fitting thermocouples and insulation. The PV cells
 230 were cut to size using Ulster University's specialist high velocity ceramic disc cutting
 231 machine and soldered to apply tinned copper electrical tabbing. Finally, the absorber
 232 surface was painted, the PV cells strings were assembled, and mounted, encapsulating
 233 resin was cast in place, and power cables were connected as illustrated on
 234 Figures 3 & 5. Unfortunately, despite care being taken to protect the PV, damage was
 235 sustained to several cells in the process of fixing and casting them in place.

236 **Table 1: Key properties of the BIPV-PLVTD-ICSSWH prototype**

Quantity	Value	Unit	Basis
Volume of water in storage tank (u)	0.1	m ³	Typical tank size reported in literature* on ICSSWH systems
Aperture and absorber area (A_1)	1	m ²	Typical absorber size reported in literature* on ICSSWH systems
PV cell coverage of absorber area (A_0)	0.75	m ²	15 strings, each formed of 8 quarter-cell pieces (78x78mm)
Absorber laminate thickness (x_{15})	5	mm	Absorber laminate consisted of PV cells cast in transparent crystal-clear silicone resin (nominal 2mm overall thickness). Resin was bonded to stainless steel substrate and faced with 3mm transparent acrylic sheet
Removeable transparent cover thickness (x_{56})	33	mm	Comprising of 3mm transparent acrylic sheet mounted on a polystyrene foam frame to form 30mm air gap between absorber and cover
Depth of PLVTD (x_{12})	70	mm	Dimension as discussed by Pugsley et al. (2020)
Depth of tank (x_3)	100	mm	Tank volume divided by absorber area
Standard power output of PV cell (q_{STC})	4.24	W	156x156mm pseudo square mc-si M-2BB solar PV cell (Bosch, 2010)

237 *The reader is directed to the literature review presented in our study introduction paper (Part 1 of 2)

238

239 **3.2 Experimental method**

240 The aim of the experimental work was to investigate the behaviour of the whole BIPV-
 241 PLVTD-ICSSWH prototype collector under representative operating conditions to
 242 validate expected behaviours predicted by the theoretical model in terms of solar
 243 thermal and photovoltaic collection efficiencies, overnight heat retention, and diurnal
 244 thermal efficiency. The thermal test experimental methodology largely follows the
 245 precedents set by Smyth et al. (2003, 2015, 2018 & 2019) and Muhumuza et al. (2019)
 246 whereby the prototype is exposed to constant simulated solar irradiance before being
 247 left to cool overnight. Most previously documented solar simulator tests on ICSSWH
 248 prototypes have covered a single 24h period whereas each test in the present work
 249 covered a 100h period corresponding to 4 consecutive days. Our preceding paper
 250 (Part 1 of 2) which introduces the present study sets out a table of insolation and
 251 average irradiance levels for three contrasting climate locations (Belfast, UK; Rome,
 252 Italy; Riyadh, Saudi Arabia) at different latitudes based on 22 years of extra-terrestrial
 253 solar radiation measurements and earth surface satellite imagery (NASA, 2019;
 254 Stackhouse et al., 2018). Equator-facing vertical surfaces such as building facades

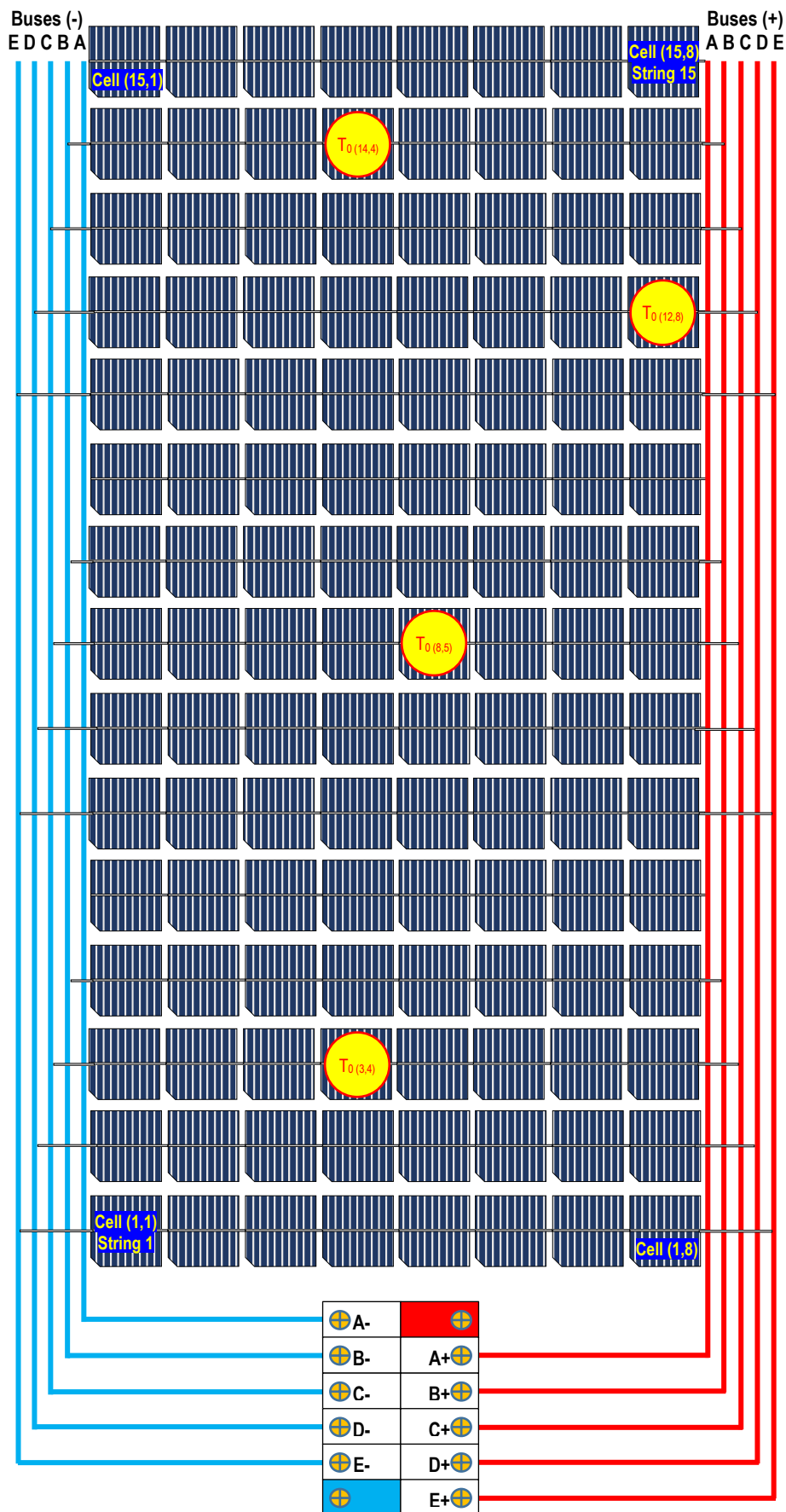
255 (assuming no shading) in Rome receive $H_{24} \approx 12 \text{ MJ/m}^2$ during both summertime and
256 wintertime periods. Lower vertical plane insolation values typically occur in Riyadh
257 during summer ($H_{24} \approx 7 \text{ MJ/m}^2$ due to the acute incident angles associated with high
258 solar altitudes) and also in Belfast ($H_{24} \approx 9 \text{ MJ/m}^2$ in summer and $H_{24} \approx 4 \text{ MJ/m}^2$ in winter
259 owing to the predominantly cloudy local climate). Higher vertical plane insolation
260 values are common in Riyadh during winter ($H_{24} \approx 14 \text{ MJ/m}^2$) and at the spring and
261 autumn equinoxes in Rome where $H_{24} \approx 20 \text{ MJ/m}^2$) occurs on the sunniest days. In order
262 to be representative of the stable mid-range insolation conditions in Rome and to
263 account broadly for the typical minima and maxima, the following four separate 100h
264 tests were undertaken:

- 265 1) Moderate daily insolation ($H_{24} = 13.2 \text{ MJ/m}^2$) with a transparent cover.
- 266 2) Moderate daily insolation ($H_{24} = 13.2 \text{ MJ/m}^2$) without a transparent cover.
- 267 3) Low daily insolation ($H_{24} = 8.0 \text{ MJ/m}^2$) without transparent cover.
- 268 4) High daily insolation ($H_{24} = 18.8 \text{ MJ/m}^2$) without transparent cover.

269 These daily insolation scenarios were simulated using 6h periods of exposure to
270 columnated vertical plane irradiance of $G = 370, 610$ and 870 W/m^2 (for low, moderate
271 and high insolation scenarios respectively) incident on the prototype at an angle
272 normal to the aperture plane. Irradiance was provided by the Ulster University solar
273 simulator (Zacharopoulos et al., 2009; Arya et al., 2018) which consists of 35 metal
274 halide lamps fitted with columnating lenses providing illumination uniformity of $\pm 10\%$
275 and an infrared filter to ensure realistic daylight spectrum similar to AM1.5.

276 The prototype was instrumented with 50 thermocouples (T-type, accuracy verified to
277 to $\pm 0.3^\circ\text{C}$) to measure temperatures of the various elements of the prototype ($T_0, T_1,$
278 T_2, T_3, T_4, T_5, T_6 and T_a as per Figure 2) and to examine planar spatial variations. The
279 majority of thermocouples were bonded to the metal body of the PLVTD or located
280 within the water storage tank (see Figure 4) although some were attached to the rear
281 of the PV cells (labelled according to cell number on Figure 3 as $T_{0(y,x)}$ where $y =$ row
282 number of string and $x =$ cell column number) and embedded within the absorber
283 laminate or fixed to the insulation and transparent cover elements (see Figures 3 & 6).
284 Temperature readings were made using a datalogger (Delta-T DL2e) set to record
285 every 5 minutes.

286

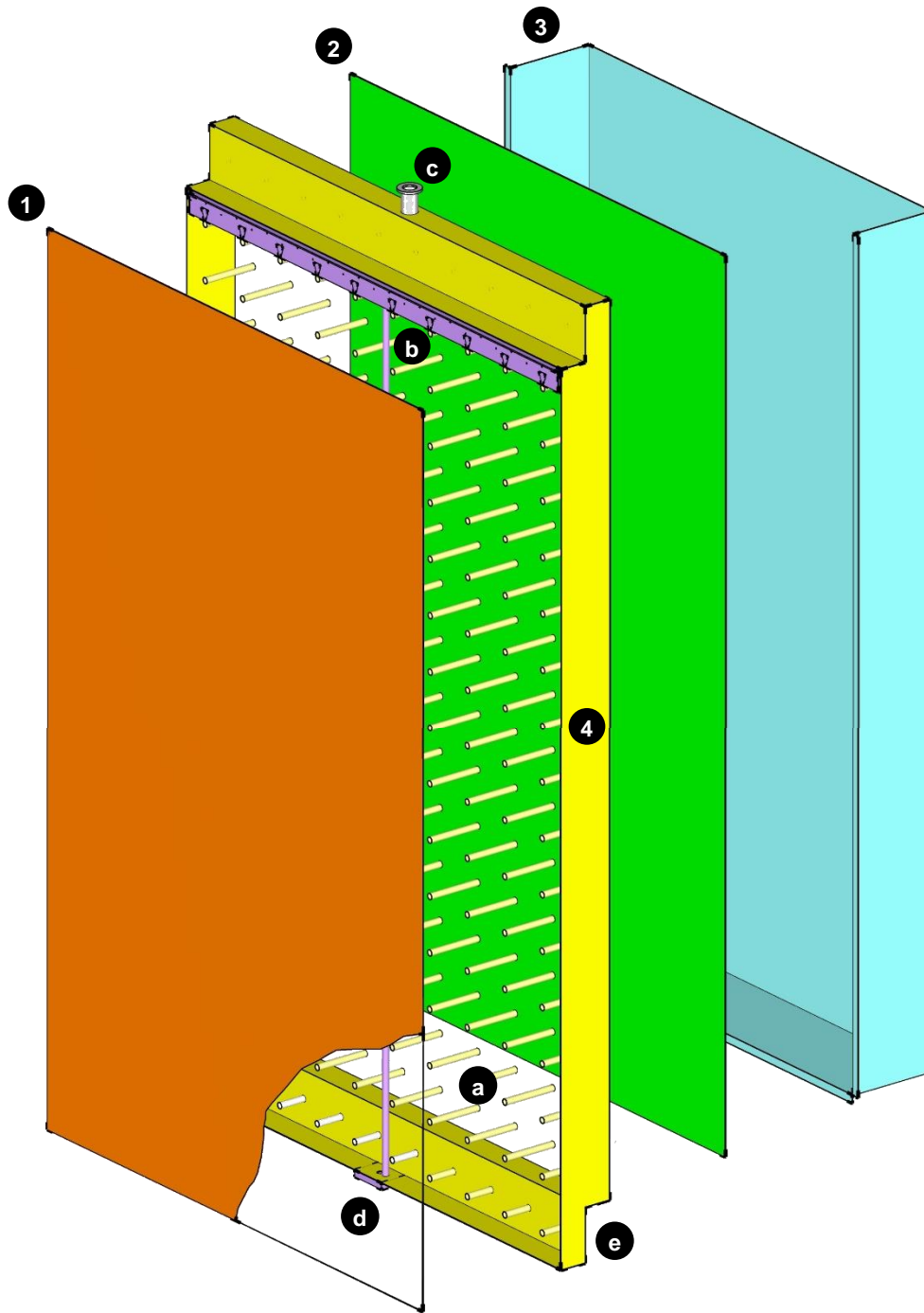


287

288 PV cell temperature measurement locations are denoted by $T_0(y,x)$ where y = row number of string and x = cell column number

289

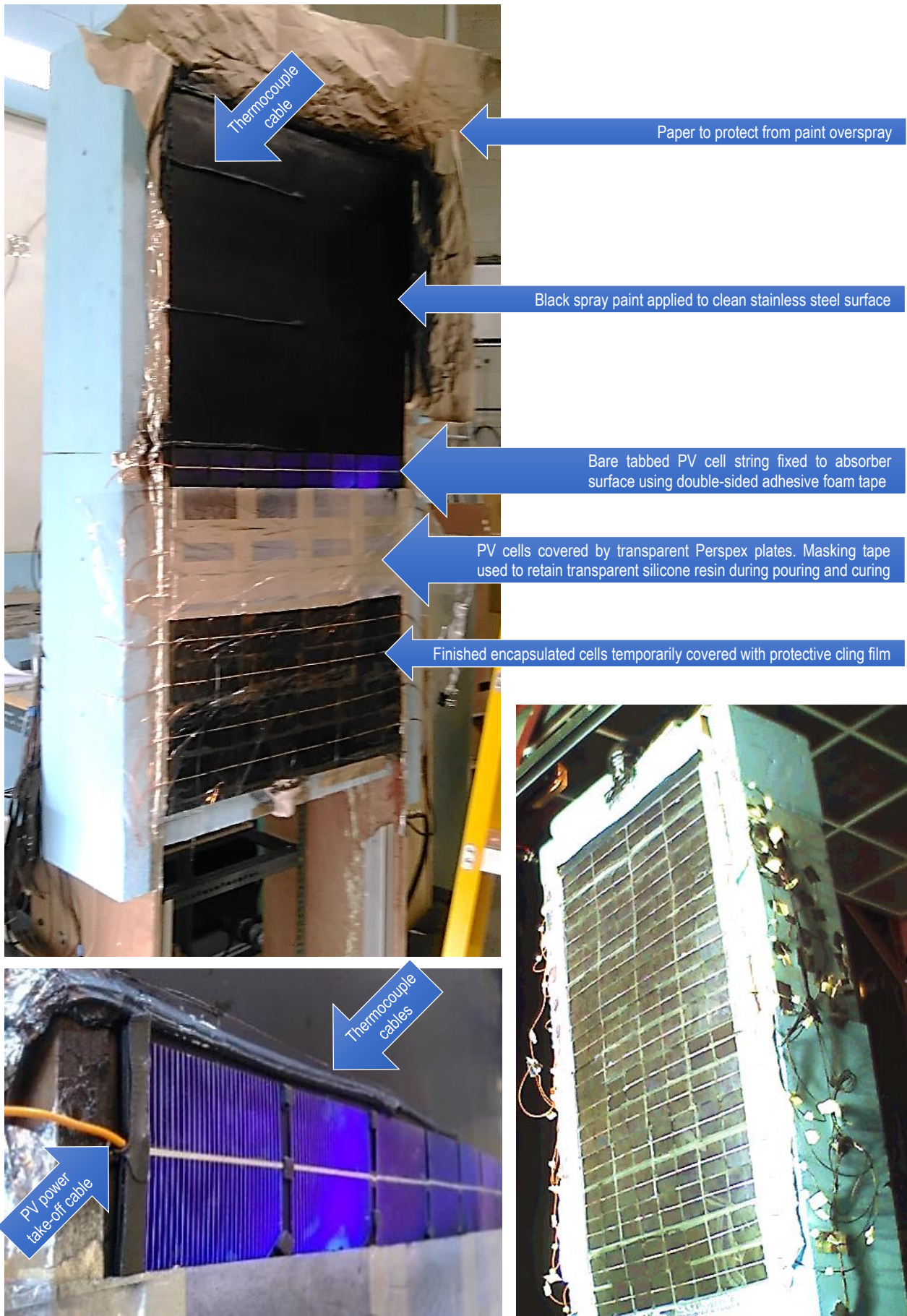
290 *Figure 3: Photovoltaic cell layout, series parallel wiring arrangement, and temperature measurement locations*



- 1) Absorber-Evaporator plate (12 thermocouples bonded to front surface to measure temperature T_1)
- 2) Condenser-tank plate (12 thermocouples bonded to rear surface to measure temperature T_2)
- 3) Water storage tank back, sides and base (5 submerged thermocouples measuring T_3)
- 4) Sidewalls forming the top, bottom and sides of the PLVTD envelope (5 thermocouples bonded to measure temperature T_4)
- a) Array of tubular struts forming internal structure
- b) Evaporator wetter distributor and diffuser nozzle
- c) Spigot for vacuum pump connection and working fluid injection
- d) Evaporator wetter pump mounting plate
- e) Working fluid reservoir with thermal break separating from condenser plate

291

292 *Figure 4: Exploded view of the PLVTD and water tank*

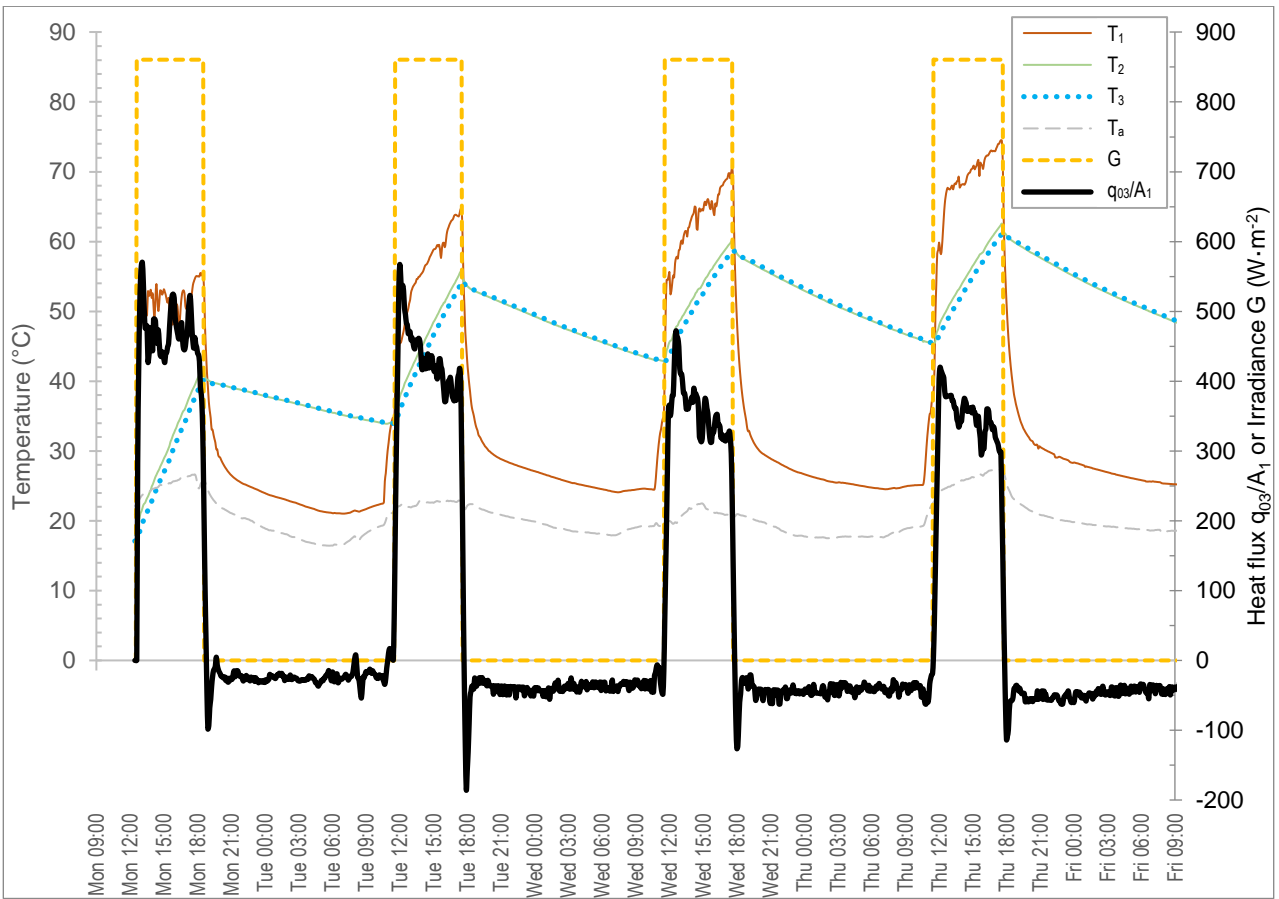


293 **Figure 5: Photos showing PV/T absorber fabrication: All process stages (Top); Bare PV cells & cables (Left) Complete prototype (Right)**
 294

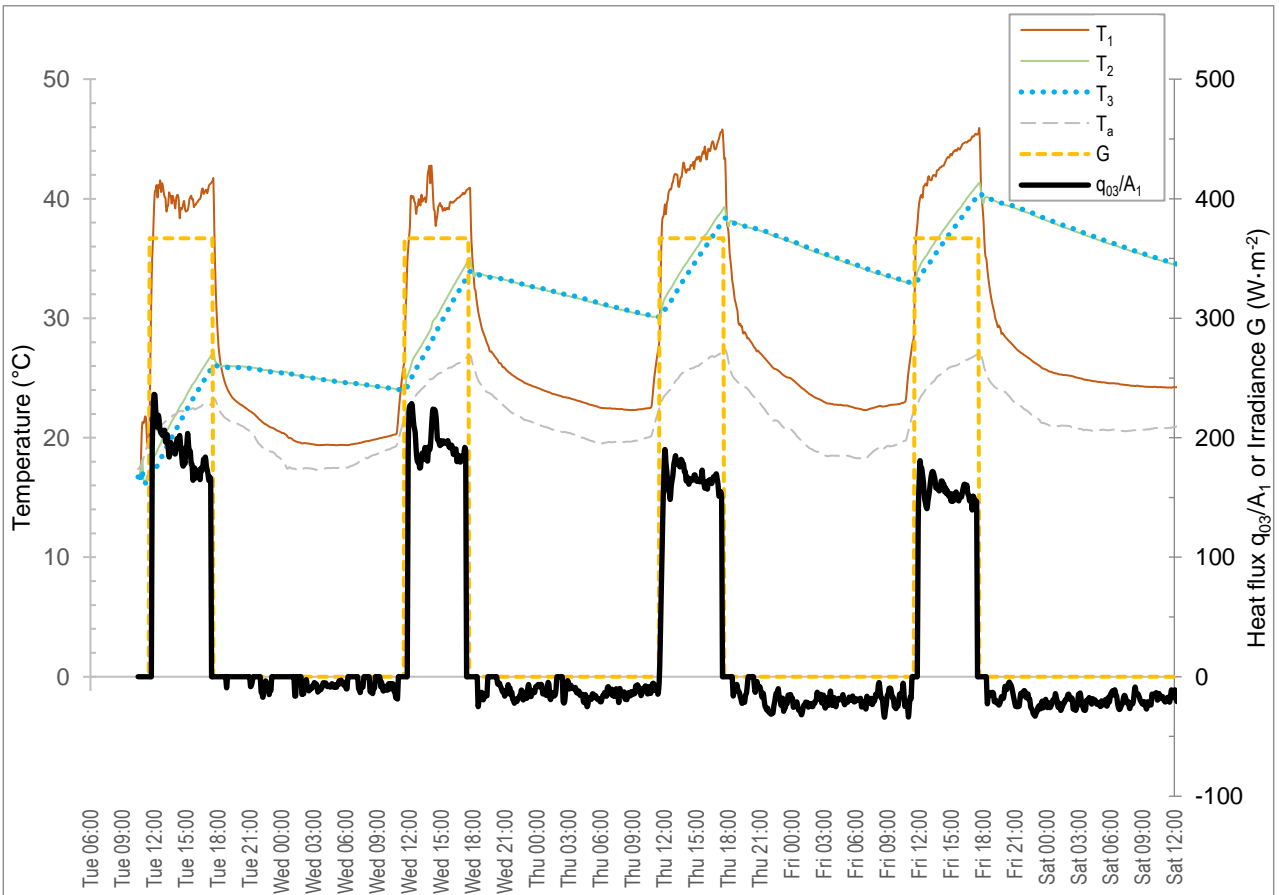
295 The storage tank temperature (T_3) changes with time (t) and was used to calculate the
296 instantaneous thermal power (q_3) delivered to or lost from the tank based on the
297 relationship $q_3 = M \cdot c_p \cdot \Delta T_3 / t_{col}$. Initial tests were undertaken to determine thermal
298 conductance of the insulated water storage tank and PLVTD sidewalls by covering the
299 evaporator plate with 300mm of insulation, filling the tank with water at 70°C, and
300 measuring the time taken to cool to $T_a=23^\circ\text{C}$ room temperature. Measurement results
301 suggested residual heat loss of $U_{3a}=1.1 \text{ W}\cdot\text{m}^{-2}\text{K}^{-1}$ over an area of $A_{3ia}=2.3 \text{ m}^2$
302 decreasing with time to $U_{3a}=0.6 \text{ W}\cdot\text{m}^{-2}\text{K}^{-1}$ as the tank temperature reduced towards
303 ambient. Having quantified residual heat losses, the instantaneous heat fluxes through
304 the absorber and thermal diode (q_{03}/A_1) and lost from absorber to ambient (q_{0a}/A_1)
305 could be calculated with reference to the energy balance model (refer to our study
306 introduction paper, Part 1 of 2). Tests were undertaken with the PV elements coupled
307 to an electrical load throughout (load resistance was adjusted periodically to ensure
308 maximum power point operation) but without any thermal load (no water draw-offs,
309 to simulate multi-day stagnation behaviour). The electrical load was temporarily
310 disconnected every 2 hours during each collection period (for about 5 minutes on each
311 occasion) to permit sampling of the PV module current-voltage characteristics using a
312 Daystar DS1000 curve tracer which automatically sweeps the load condition from I_{sc}
313 to V_{oc} through the maximum power point operating condition ($q_{E,mpp}$). Supplementary
314 measurement equipment included a calibrated pyranometer (Kipp & Zonen CM4) to
315 measure irradiance levels; two Digital Multimeters (Amprobe AM-510-EUR) to monitor
316 photovoltaic currents and voltages and measure load resistance; an Infrared
317 Thermometer (Fluke 561) and a Thermal Imaging Camera (Testo 875-1i) to measure
318 absorber surface temperatures. The experimental procedure is detailed in full by
319 Pugsley (2017) but is not repeated here for the sake of brevity.

320 **3.3 Solar thermal collection and heat retention results**

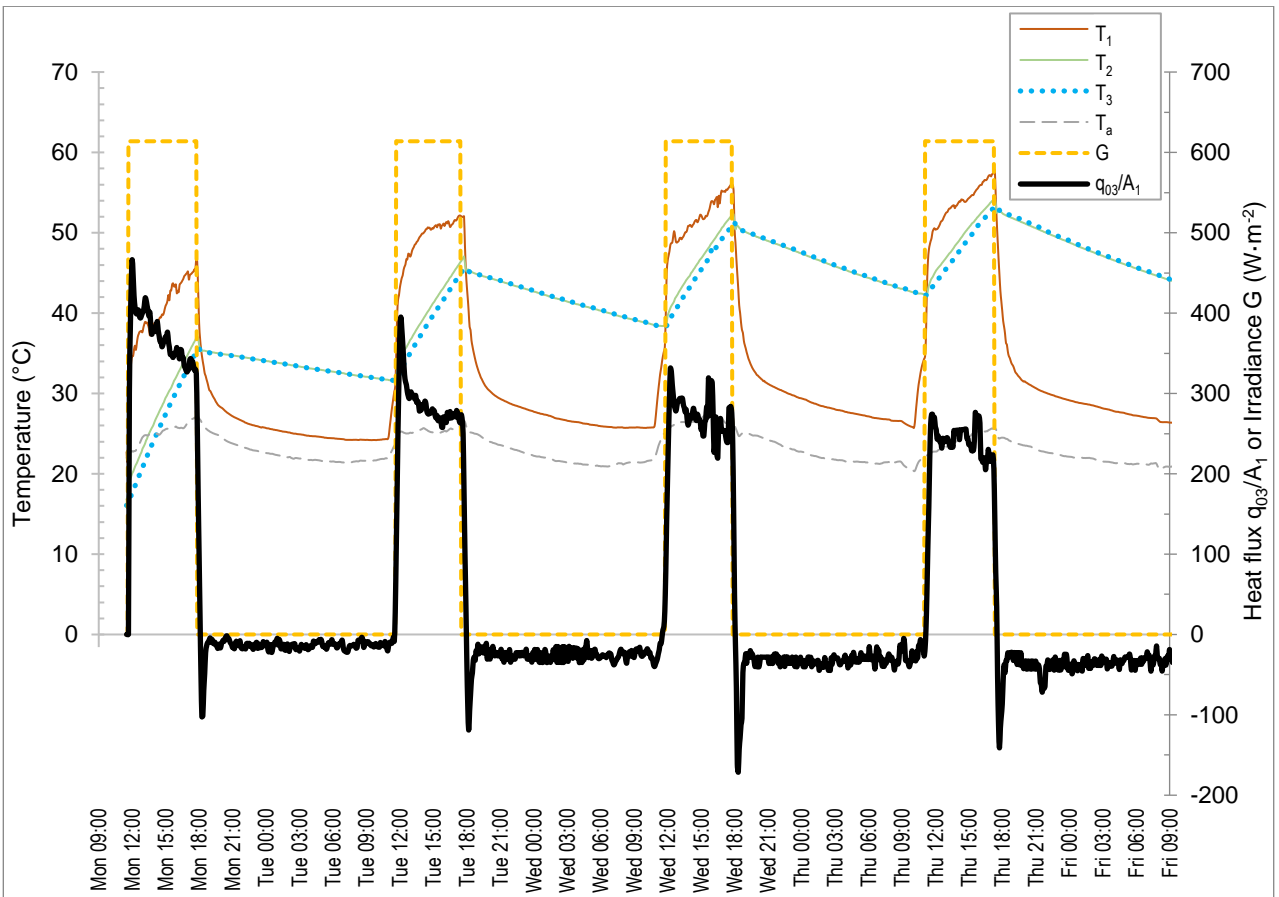
321 Temperature time histories with corresponding solar irradiances and absorber heat
322 fluxes are shown on Figures 6 to 9 for each of the multi-day tests. Solar heat collection
323 is apparent when the prototype is exposed to irradiance which causes the absorber-
324 evaporator plate temperature (T_1) to rise and for heat flux ($150 < q_{03}/A_1 < 600 \text{ W}\cdot\text{m}^{-2}$)
325 to be transmitted to the condenser-tank plate (T_2) across the PLVTD temperature
326 difference ($3 < \Delta T_{12} < 30^\circ\text{C}$) causing a steady increase in water storage tank
327 temperature from the starting condition $T_3 \approx T_a \approx 17^\circ\text{C}$.



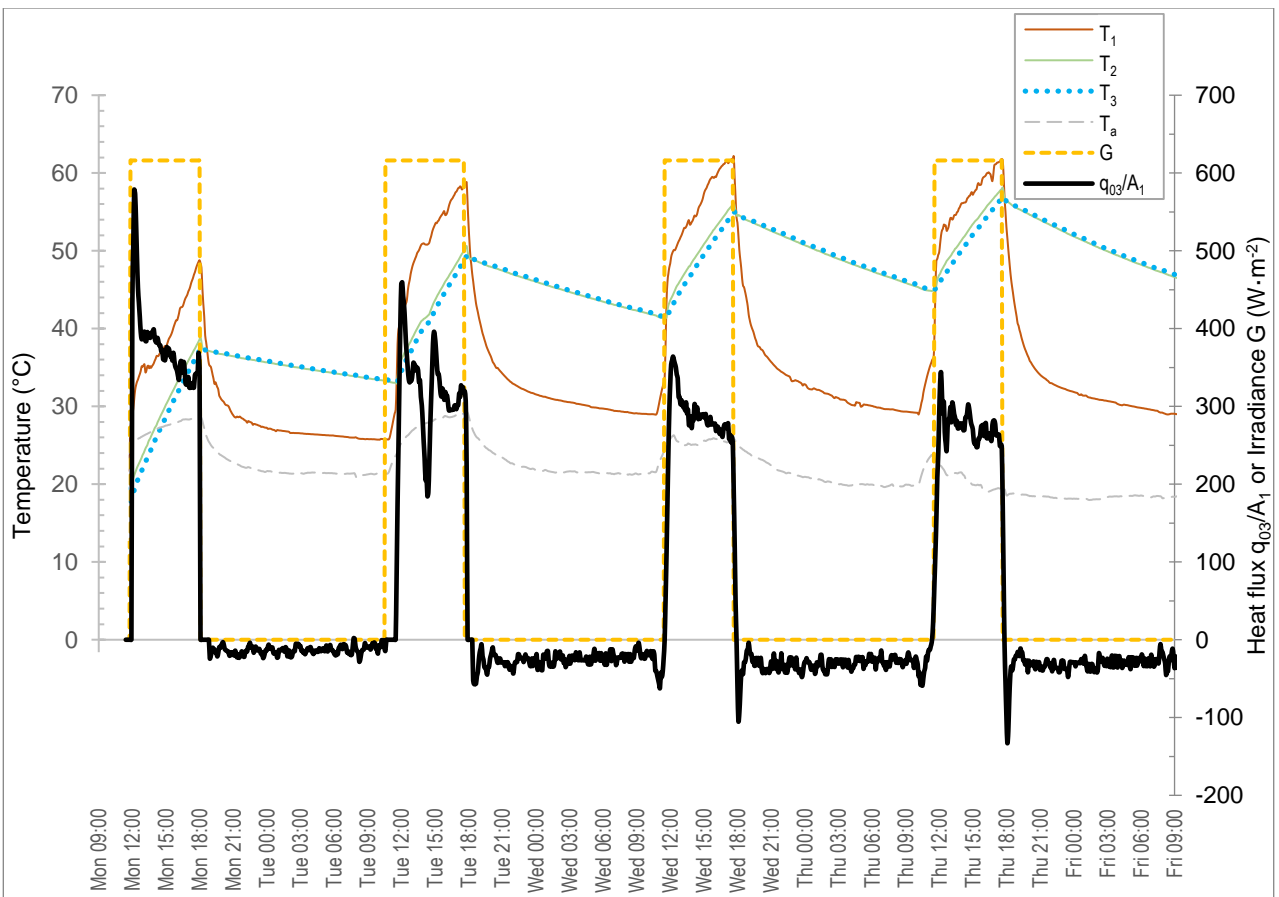
328
329 **Figure 6: Temperature and heat flux time history results for tests under high irradiance without absorber transparent cover**



330
331 **Figure 7: Temperature and heat flux time history results for tests under low irradiance without absorber transparent cover**



332
333 **Figure 8: Temperature and heat flux time history results for tests under moderate irradiance without absorber transparent cover**



334
335 **Figure 9: Temperature and heat flux time history results for tests under moderate irradiance with absorber transparent cover**

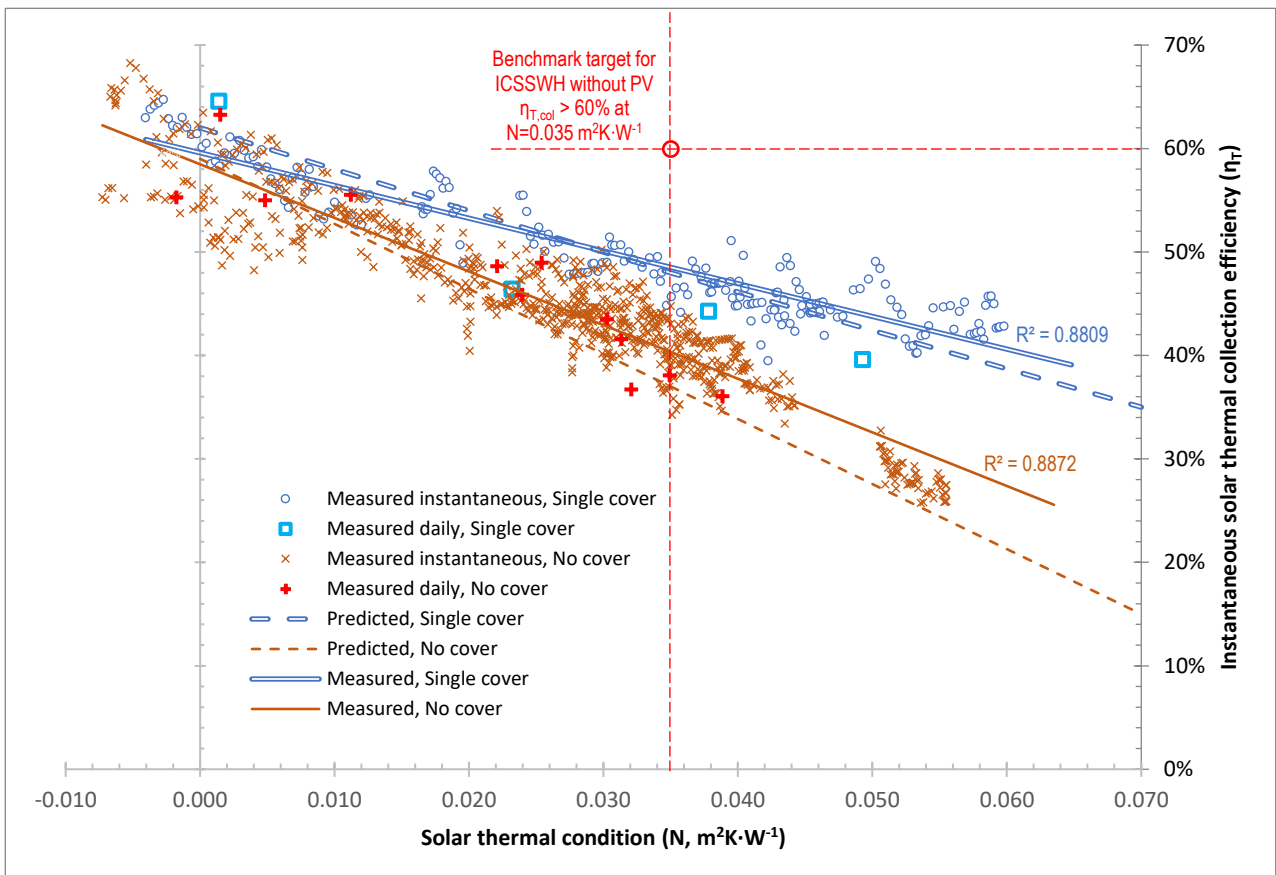
336 Retention periods occur when irradiance ceases ($G=0$) causing absorber-evaporator
337 plate temperatures to fall below those of the condenser-tank plate ($5 < -\Delta T_{12} < 25^\circ\text{C}$)
338 and for a steady heat loss flux ($15 < -q_{03}/A_1 < 60 \text{ W}\cdot\text{m}^{-2}$) to develop causing a steady
339 decrease in T_3 . As discussed by Pugsley et al. (2020), the measured heat fluxes and
340 temperature differences imply thermal diode conductances of $U_{f,12} \approx 38 \text{ W}\cdot\text{m}^{-2}\text{K}^{-1}$ in
341 forward (collection) mode and $U_{r,12} = 1.7 \text{ W}\cdot\text{m}^{-2}\text{K}^{-1}$ in reverse (retention) mode.

342 Water storage tank temperatures were observed to reach maxima of $T_3 = \tilde{T}_a + 34 =$
343 61°C and $T_3 = \tilde{T}_a + 15 = 40^\circ\text{C}$ by the end of Day 4 respectively for the high and low
344 irradiance tests without transparent cover (see Figures 6 and 7). Day 4 maximum
345 temperatures for the moderate irradiance tests without and with the transparent cover
346 (see Figures 8 & 9) were respectively $T_3 = \tilde{T}_a + 29 = 53^\circ\text{C}$ and $T_3 = \tilde{T}_a + 34.8 = 57^\circ\text{C}$
347 which shows the beneficial effect of reducing absorber heat losses. These test results
348 (obtained for $H_{24} = 13.2 \text{ MJ}/\text{m}^2$ without wind) correspond reasonably closely to the
349 theoretical modelling (refer to Figure 9 of our study introduction paper, Part 1 of 2)
350 which predicted a Day 4 maximum temperature of $T_3 = \tilde{T}_a + 29.2 = 51.2^\circ\text{C}$ for Variant B
351 which is representative of a BIPV-PLVTD-ICSSWH with single transparent cover
352 operating under average summertime conditions in Rome ($H_{24} = 11.5 \text{ MJ}/\text{m}^2$ with $2 \text{ m}/\text{s}$
353 wind). This provides reasonable validation of the model when allowing for minor
354 differences in insolation and the absence of wind during tests.

355 The measured instantaneous and daily solar thermal collection efficiencies are
356 presented on Figure 10. Based on least-squares regression lines ($R^2 > 0.88$) fitted to
357 the measured data, the zero-loss performances ($N = 0 \text{ m}^2\text{K}\cdot\text{W}^{-1}$) of the bare absorber
358 and single covered variants of the BIPV-PLVTD-ICSSWH collector are $\eta_T = 58\%$ and 60%
359 respectively. Measured performances at the benchmark solar thermal condition
360 ($N = 0.035 \text{ m}^2\text{K}\cdot\text{W}^{-1}$) are $\eta_T = 40\%$ and 49% respectively, somewhat lower than the
361 $\eta_T = 60\%$ target for state-of-the-art ICSSWH collectors as expected, due to some of the
362 incident energy ($\sim 10\%$) being converted to electricity rather than heat. Measured
363 trends are in reasonable agreement with predicted performances which provides
364 further model validation. Small discrepancies between modelled and measured results
365 are primarily associated with the thermal diode conductance which was modelled as
366 constant $U_{f,12} \approx 38 \text{ W}\cdot\text{m}^{-2}\text{K}^{-1}$ but varied in practice (95% of values varied in the range

367 $\pm 17 \text{ W}\cdot\text{m}^{-2}\text{K}^{-1}$ as reflected by the scatter in the measured data) owing to its
 368 temperature and heat flux dependence (refer to Pugsley et al., 2020). It should be
 369 noted that data on Figure 10 excludes transients during the first 30 minutes of each
 370 collection period when the rise in tank temperature occurs very much slower than the
 371 rise in absorber temperature owing to the lag introduced by the latent thermal mass
 372 associated with liquid-vapour phase change within the PLVTD. Apparent instantaneous
 373 solar thermal efficiencies during these transients were typically $\sim 10\%$ lower than the
 374 steady-state values.

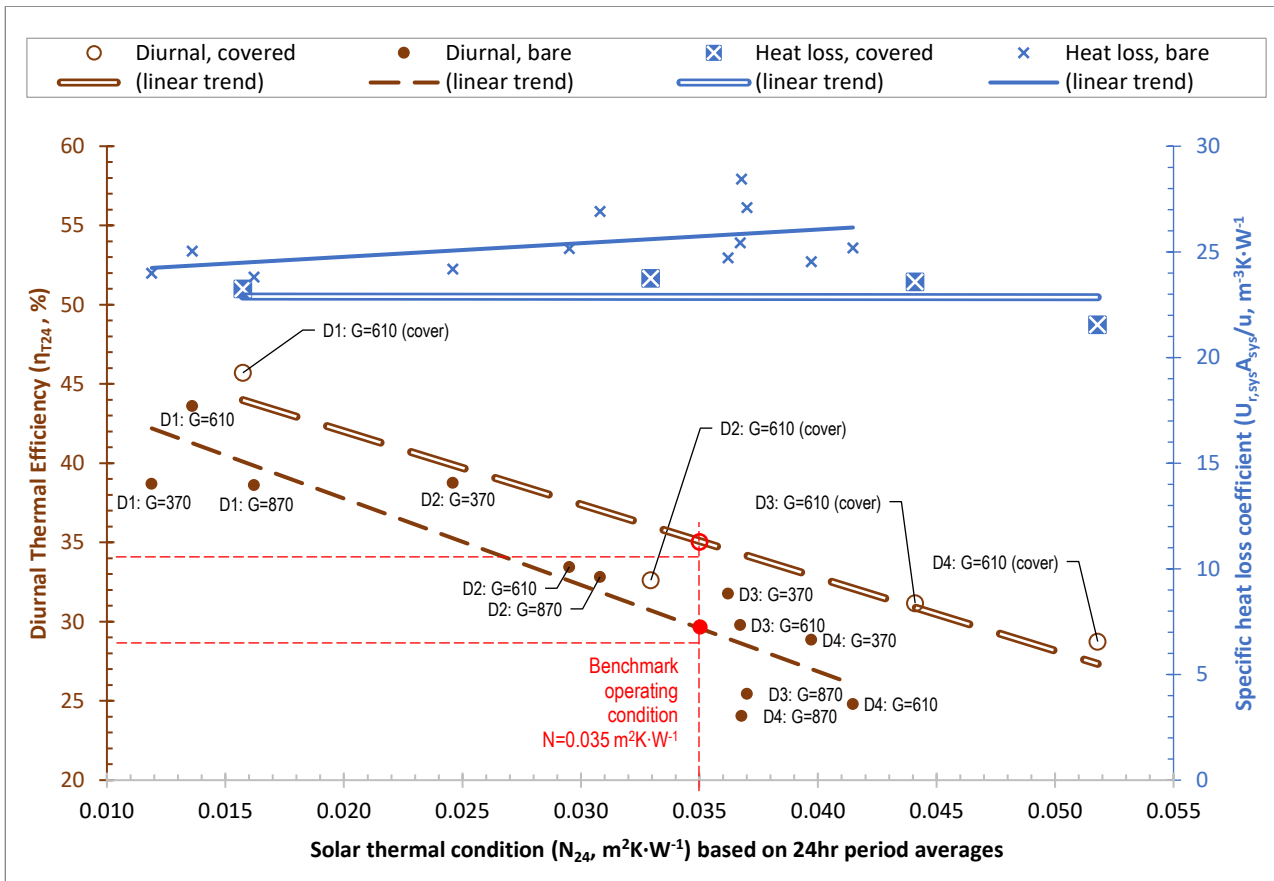
375



376

377 *Figure 10: Solar thermal collection efficiency of BIPV-PLVTD-ICSSWH prototype with and without transparent cover*

378



379
 380 *Figure 11: Measured diurnal thermal efficiencies and specific heat loss coefficients on Days D1, D2, D3 & D4 of testing*
 381

382 Measured diurnal thermal ($\eta_{T,24}$) efficiencies and volume specific heat loss coefficients
 383 ($U_{r,sys}A_{sys}/u$) are summarised on Figure 11. Whole-period results for each day (D1, D2,
 384 D3 & D4) of each test (irradiances $G = 370, 610 \text{ \& } 870 \text{ W/m}^2$ with and without cover)
 385 are presented with reference to daily solar thermal condition (N_{24} calculated according
 386 to Equation 5 based on 24h average \tilde{T}_3 and \tilde{T}_a). Results show that single covered and
 387 bare absorber variants of the BIPV-PLVTD-ICSSWH prototype achieved diurnal
 388 efficiencies of $\eta_{T,24} = 35\%$ and 29% respectively at the benchmark solar thermal
 389 condition ($N=0.035 \text{ m}^2\text{K}\cdot\text{W}^{-1}$) which is in good agreement with model predictions.

390 Measured heat loss coefficients were $U_{r,sys}A_{sys}/u = 25.4$ and $23.0 \text{ W}\cdot\text{m}^{-3}\text{K}^{-1}$ respectively
 391 for the bare absorber and single covered variants of the BIPV-PLVTD-ICSSWH,
 392 corresponding to 18h heat retention efficiencies of $\eta_{ret} = 71\%$ and 69% respectively.
 393 These values are broadly similar to those predicted by the theoretical model ($U_{r,sys}A_{sys}/u$
 394 $\approx 20 \text{ W}\cdot\text{m}^{-3}\text{K}^{-1}$, refer to our study introduction paper, Part 1 of 2) and as expected, do
 395 not exhibit significant dependence upon temperature within the ranges examined. As
 396 predicted by the modelling results the heat loss coefficients demonstrate that the
 397 transparent cover provides only a small benefit ($\sim 10\%$ $U_{r,sys}$ improvement or $\sim 2\%$

398 extra η_{ret}) in respect of controlling overnight heat loss when used in tandem with a
399 PLVTD. The model suggests that the cover would have a much larger effect if no PLVTD
400 were employed which is why most ICSSWH collectors (which do incorporate thermal
401 diodes) employ one or more transparent covers to control overnight heat loss.

402 **3.4 Photovoltaic performance results**

403 Measured open circuit voltages, short circuit currents, and fill factors for each string
404 are shown on Figure 12. The same data for the whole module (formed by connecting
405 the strings as a 5x series by 3x parallel module, see Figure 3 and discussion in
406 Section 3.1) is shown on Figure 13.

407 Open circuit voltage under moderate to high irradiance conditions varied from
408 $V_{\text{oc}}=4.75\pm 0.07$ V per string at 25°C to a little less than 4V at 70°C (Figure 12a) and
409 the maximum measured overall module open circuit voltage was $V_{\text{oc}} = 5 \times 4.75 = 24\text{V}$
410 (Figure 13). Corresponding voltage-temperature coefficients ($K_{V:T} = -0.36\%/K$ for
411 strings and $K_{V:T} = -0.38\%/K$ for whole module) are very close to the manufacturers
412 published data (single cell $K_{V:T} = -0.37\%/K$ according to Bosch, 2010). A slight drop in
413 open circuit voltage is apparent under low irradiance ($G=370$ W/m²), corresponding to
414 voltage-irradiance coefficient of $K_{V:G} \approx 96\%$, broadly as expected.

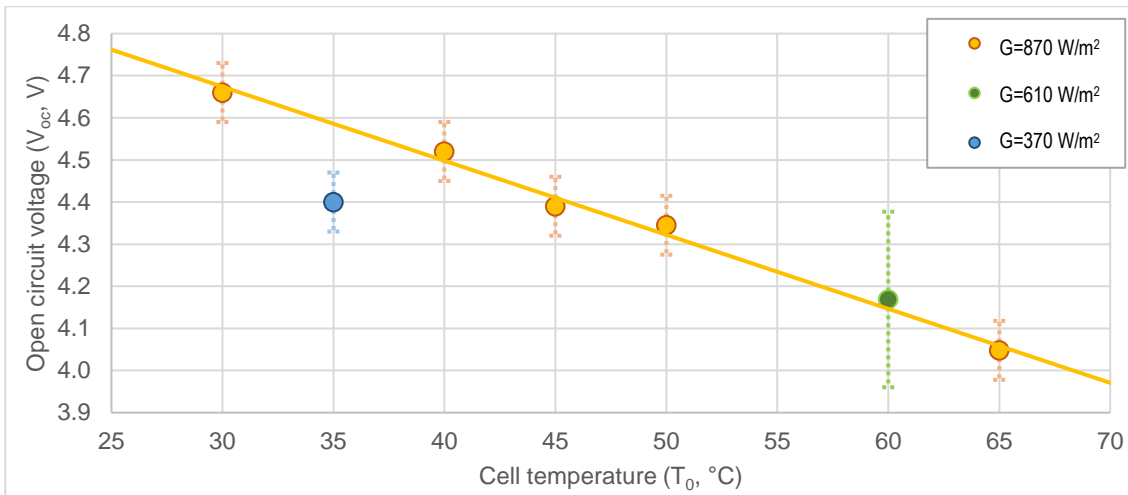
415 Short circuit currents varied from $I_{\text{sc}} = 0.4\text{A}$ for the worst string under low irradiance
416 up to $I_{\text{sc}} = 1.7\text{A}$ for the best string, and $I_{\text{sc}} = 4.5$ A for the whole module, under high
417 irradiance ($G=870$ W/m²). Calculated current-intensity relationships for individual
418 strings were found to be in the range $23 < I_{\text{sc}}/(G \cdot A) < 40$ mA/W which is lower than
419 the expected 45 mA/W implied by manufacturer's performance data (Bosch, 2010).
420 This is largely attributed to partial delamination of the bonded transparent covers
421 (which gave cells a slightly whitened or faded appearance, implying optical losses) and
422 also due to accidental cell damage (cracks etc which reduce active collection area and
423 introduce electrical resistances). Comparison of short circuit currents measured on
424 20 & 25 May against those measured on 16 May (see Figure 12b) clearly indicates a
425 performance drop for Strings 2 & 3 which is consistent with cells having suffered
426 permanent damage such as thermo-mechanical stresses causing cells to crack. Smaller
427 performance drops are also evident for Strings 1, 8, 9 and 10 and are consistent with
428 optical losses caused by cover delamination. Whole-module test data (Figure 13)
429 indicates that the current-temperature effect is $K_{I:T} \approx -0.04\%/K$ (based on trendline
430 gradients) or $K_{I:T} \approx -0.07\%/K$ (across the temperature range) with an abrupt non-linear

431 step in behaviour at a critical temperature ($T_1 \approx 50^\circ\text{C}$ for most tests but $T_1 \approx 70^\circ\text{C}$ for
432 the high irradiance test). Current-temperature effects are usually linear and of
433 relatively small positive magnitudes ($K_{I:T} \approx +0.03\%/K$ expected for a single cell
434 according to Bosch, 2010) but in this case the effect is significantly negative and non-
435 linear, consistent with PV cell fractures induced by thermal stress. The absorber
436 laminate is formed of a mixture of metal (thermal diode evaporator), ceramic (PV
437 cells), and polymeric (bonded transparent cover) elements which all have different
438 thermal expansion coefficients. This induces thermal stress which causes cracks to
439 form when the absorber temperature increases due to the metal and polymeric
440 elements expanding more quickly than the fragile PV cells. The cracks open when the
441 absorber is hot, which causes fractured parts of the PV cells to be electrically isolated
442 from the strings. The cracks close again when the absorber cools, allowing fractured
443 parts to reconnect to the string (albeit imperfectly).

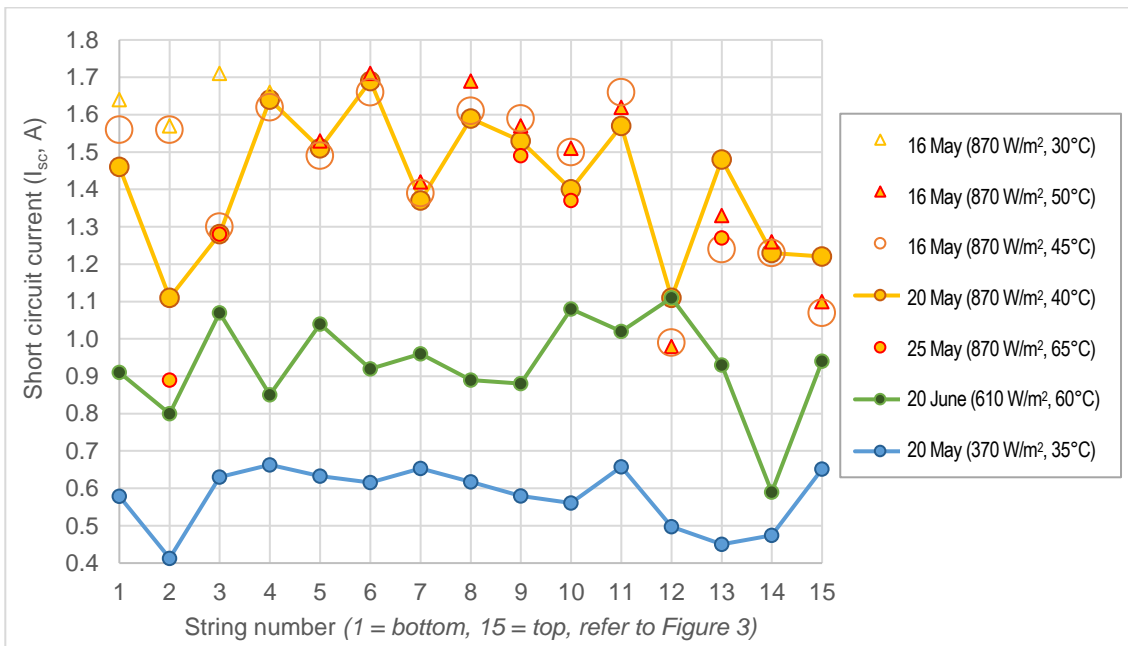
444 A typical 8-cell string achieved fill factors of $FF=74\%$ during high irradiance tests and
445 $FF=77\%$ during low irradiance tests (Figure 12) which is consistent with the typical
446 $75\% < FF < 85\%$ range reported in the literature (refer to Section 2.2 of our study
447 introduction paper, Part 1 of 2). Whole-module tests (Figure 13) exhibited a wider
448 range of measured fill factors ($66\% < FF < 81\%$) but average values were very similar
449 to those measured for individual strings. As expected, the lowest measured fill factors
450 typically correspond to the highest irradiances when series resistances (eg soldered
451 connections, tabbing, and cables) have the greatest influence. As expected, measured
452 fill factors do not appear to exhibit any significant temperature dependence.

453 Measured current-voltage and load-power curves for the whole module are presented
454 on Figures 14 & 15 respectively. As expected, voltage reduces with increasing
455 temperature and current reduces with reducing irradiance. The optimal load conditions
456 indicated by the peaks on Figure 15 were used during the experiments as a guide to
457 enable periodic adjustment of the load resistance (R_E) to ensure continuous operation
458 close to the maximum power point. The highest measured maximum power point
459 power output ($q_{E,mp} = 75\text{W}$, $FF=70\%$, $R_E=5\Omega$) occurred whilst the tank was close to its
460 lowest temperature under the high irradiance condition ($G=870\text{ W/m}^2$ without cover,
461 $T_3=17^\circ\text{C}$). The lowest measured output ($q_{E,mp}=24\text{ W}$, $FF=72\%$, $R_E=14\Omega$) occurred
462 whilst the tank was close to its maximum temperature under the low irradiance
463 condition ($G=370\text{ W/m}^2$ without cover, $T_3=40^\circ\text{C}$). Figure 14 indicates that a reduction

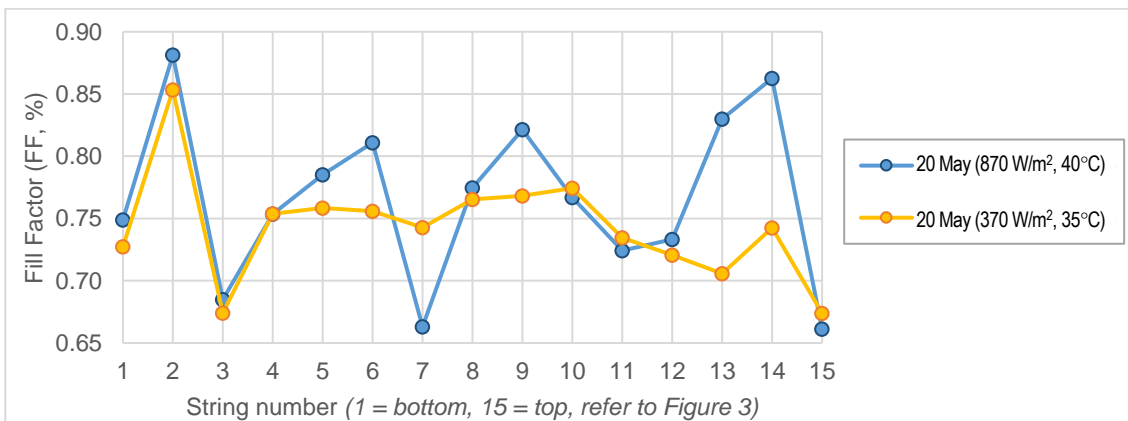
464 in I_{sc} occurs when the transparent cover is added (13% reduction for $T_3 \approx 17^\circ\text{C}$ cold
465 tank case, 6% reduction for $T_3 \approx 50^\circ\text{C}$ hot tank case) but the exact magnitude of the
466 optical loss (expected to be $\sim 8\%$) is impossible to determine owing to superimposed
467 current-temperature effects. Figure 16 shows how the maximum power point electrical
468 efficiency of the whole PV module varies with absorber temperature from maxima at
469 $T_1 \approx 25^\circ\text{C}$ of $\eta_{E,mp}$ 11.4% (without cover) and $\eta_{E,mp}$ 9.8% (with cover) to minima of
470 $\eta_{E,mp}$ 5.6% (without cover at $T_1 \approx 89^\circ\text{C}$) and $\eta_{E,mp}$ 5.9% (with cover at $T_1 \approx 62^\circ\text{C}$).
471 Measured low temperature efficiencies for the covered collector are lower than
472 expected ($\eta_{E,mp}$ 10.9% predicted by the theoretical model, refer to Figures 7 and 9 of
473 our study introduction paper, Part 1 of 2). This reduction can be explained by the
474 accidental cell damage which occurred during fabrication and by the optical losses
475 caused by partial delamination of the bonded transparent cover during initial tests.
476 Measured efficiencies at higher temperatures deviate further from model predictions
477 owing to the higher than expected current-temperature effect which appears to be
478 associated with thermal stress cracks in the PV cells (see discussion above).
479



480



481



482

483

484

485

486

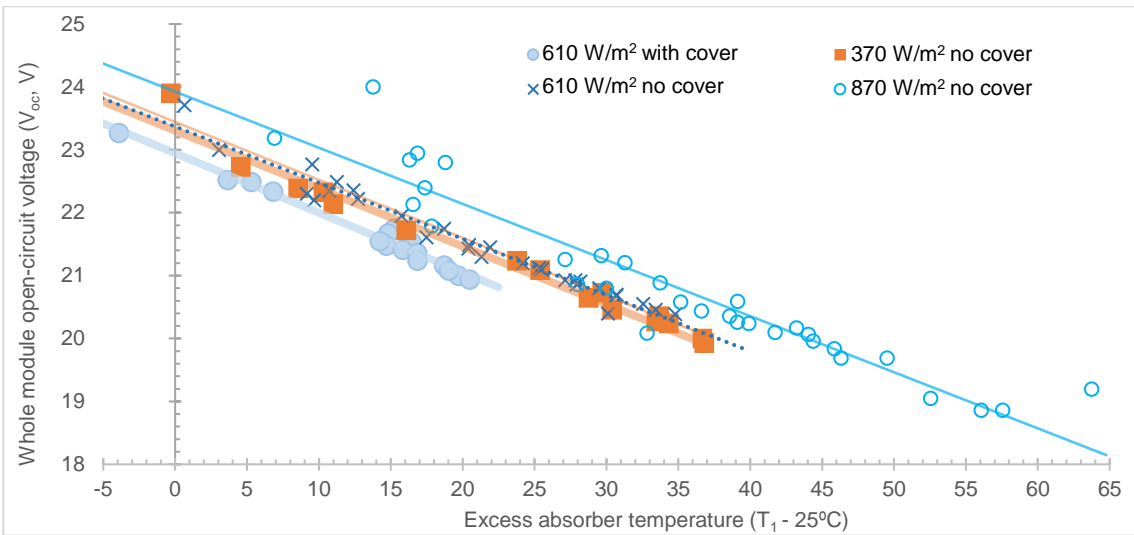
487

- a) Upper graph shows temperature dependence of average measured open circuit voltage. Vertical error bars represent the observed range of voltage variation between different strings.
- b) Middle graph compares measured short circuit currents for each string. Measurements were made at various different temperature and irradiance conditions and on various dates.
- c) Lower graph compares measured Fill Factors for each string under high and low irradiance conditions.

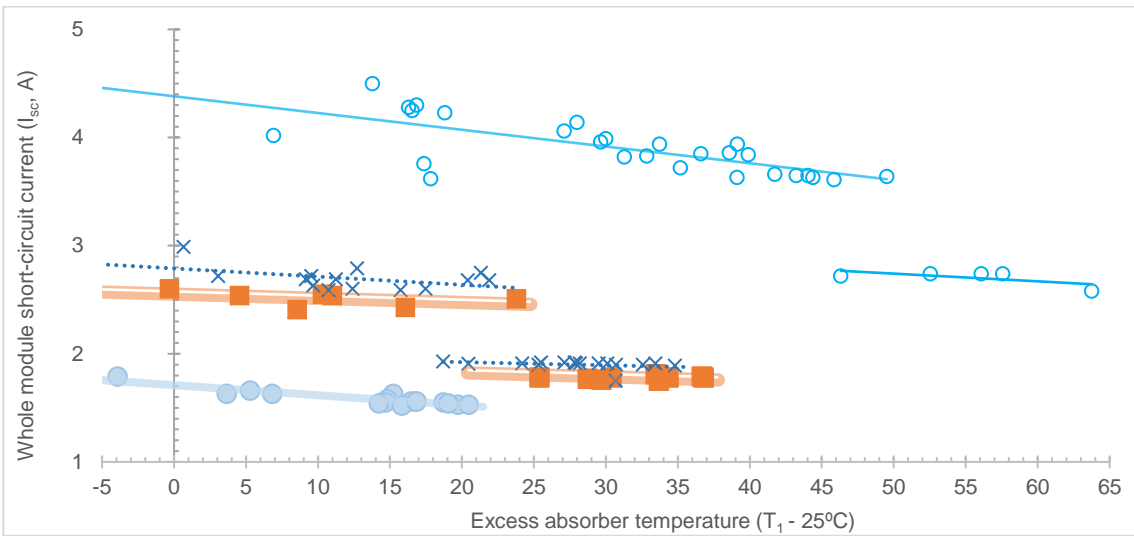
488

Figure 12: Results of photovoltaic measurements on individual 8-cell strings

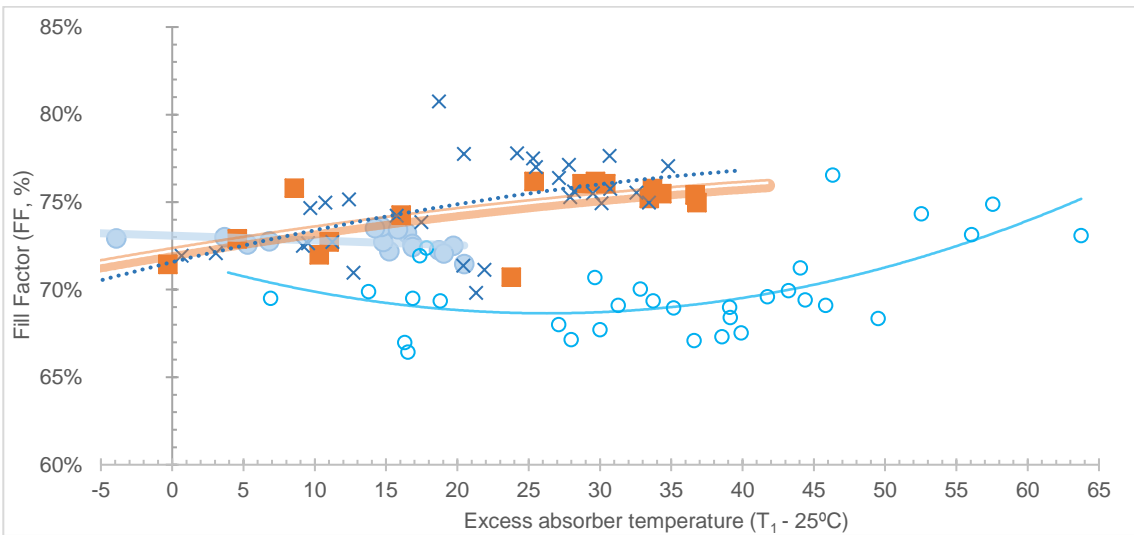
489



490



491



492

493

494

495

496

- a) Upper graph shows temperature dependence of measured open circuit voltage.
- b) Middle graph shows temperature dependence of measured short circuit current.
- c) Lower graph compares shows temperature dependence of measured Fill Factors.

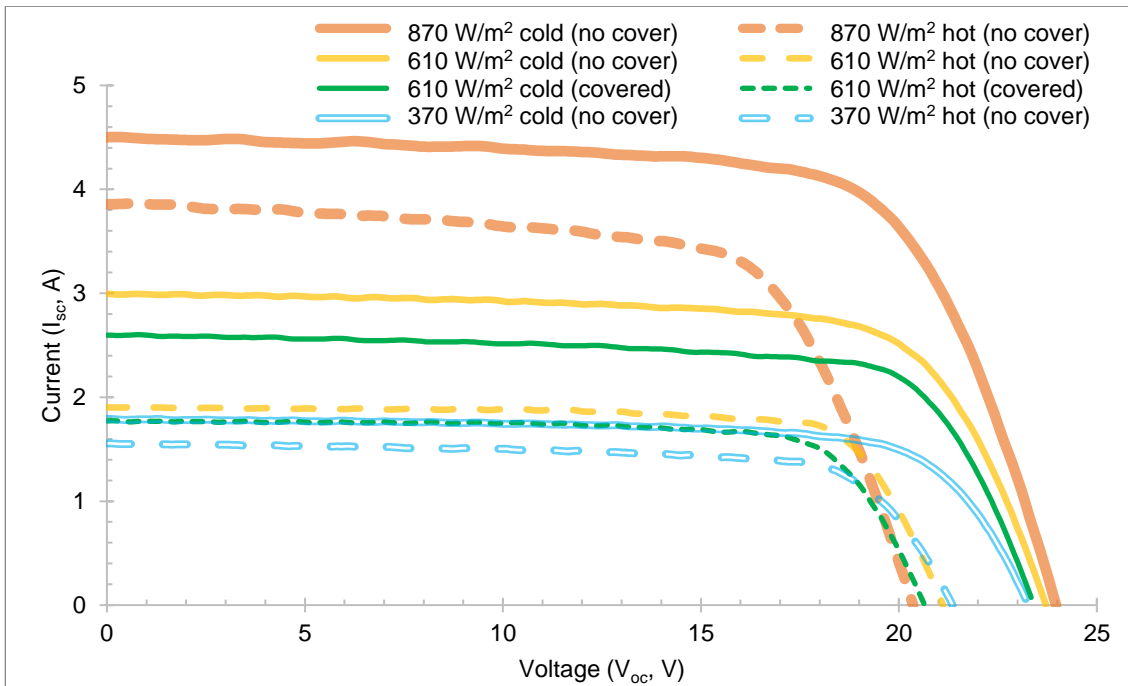
497

The x-axis corresponds to the absorber temperature less the Standard Test Condition (STC) reference temperature of 25°C.

498

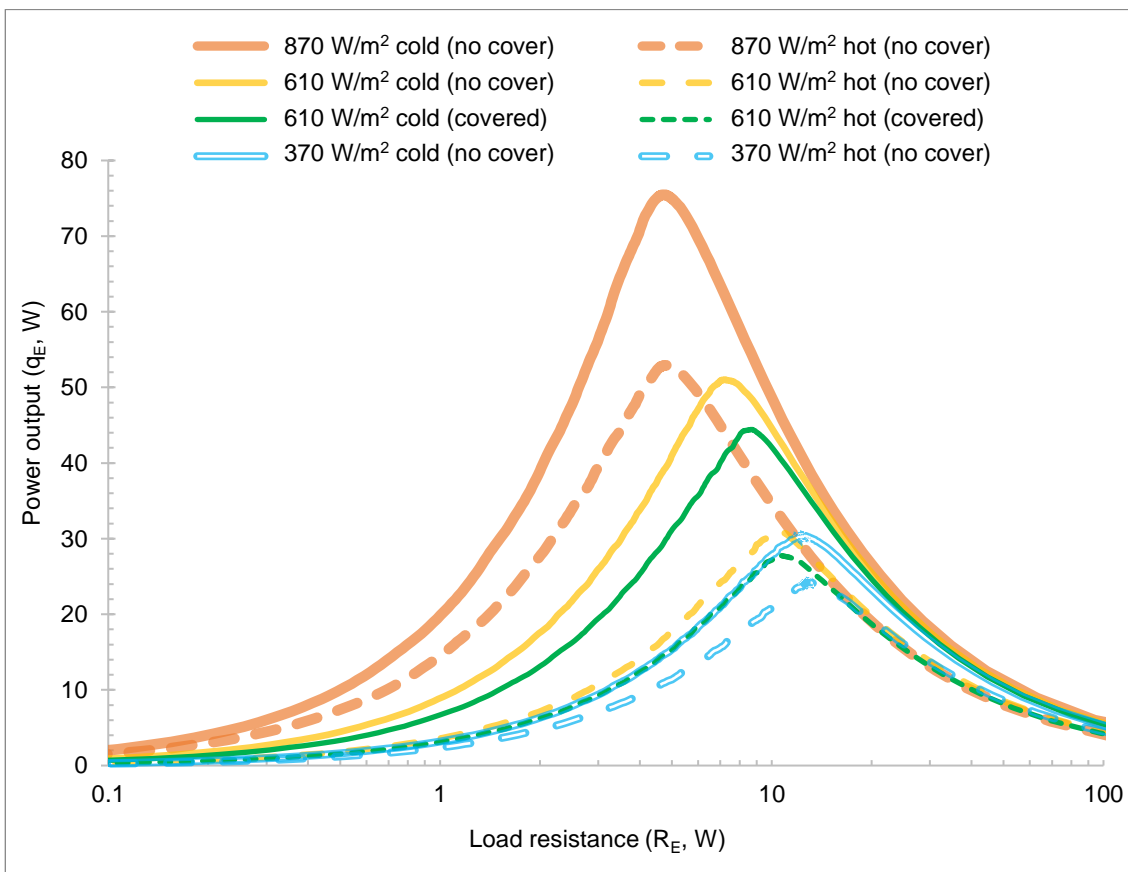
Figure 13: Results of photovoltaic measurements on the whole module

499



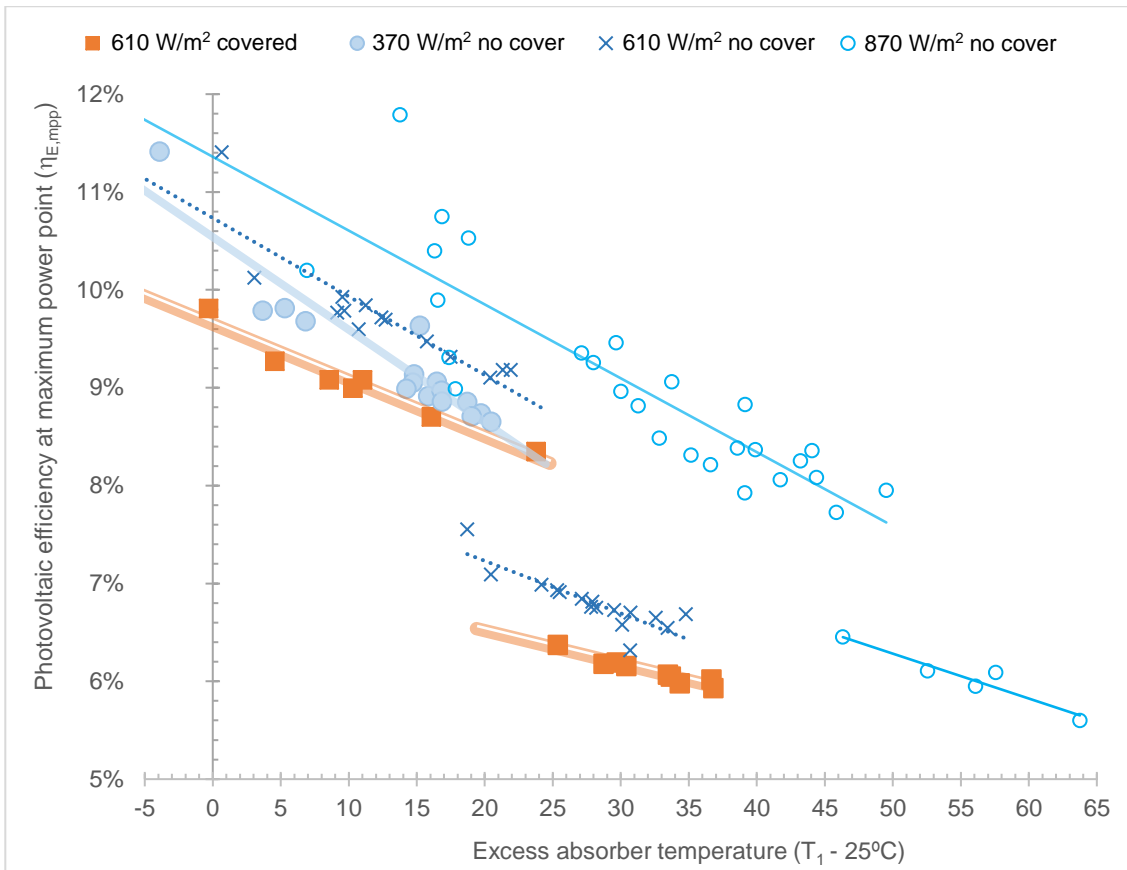
500
501
502

Figure 14: Current-voltage characteristics of the photovoltaic module under a variety of different conditions



503
504
505

Figure 15: Load-Power characteristics of the photovoltaic module under a variety of different conditions



506
 507 *Figure 16: Variation in measured maximum power point photovoltaic efficiency with temperature and irradiance*
 508

509 **3.5 Conclusions concerning model validity**

510 The measured thermal behaviour of the BIPV-PLVTD-ICSSWH prototype is in good
 511 agreement with the theoretical model. Measured maximum and minimum water
 512 storage tank temperatures are typically within $\pm 3^\circ\text{C}$ of modelled values, solar thermal
 513 collection efficiencies are typically within $\pm 3\%$ of modelled values, and specific
 514 overnight heat loss coefficients are typically within $\pm 3 \text{ W}\cdot\text{m}^{-3}\text{K}^{-1}$ of modelled values.
 515 The photovoltaic performance of the prototype was somewhat worse than expected
 516 owing to accidental damage to PV cells during fabrication and also due to delamination
 517 of the bonded transparent cover. The current-temperature relationship was the
 518 opposite of that expected and exhibited non-linearities which appear to be the result
 519 of PV cell cracks induced by thermal stress. Despite these issues, measured voltage-
 520 temperature trends, the current-irradiance relationship, and fill factors, were all
 521 broadly as expected, indicating that the core theoretical model is valid.

522

523 **4 Building integration and future concept development**

524 Development of the BIPV-PLVTD-ICSSWH approach from concept to reality requires
525 an appreciation of the available energy resource, the key operating principles, and a
526 validated theoretical understanding of device behaviour, as established through the
527 parametric modelling and experimental work presented in this two-part study. Future
528 design work and realisation of pre-commercial prototypes requires consideration of the
529 application context (such as the thermal and electrical energy demands served by the
530 system) as well as the practical constraints and opportunities associated with
531 integration into conventional architectural and building services systems.

532 **4.1 Building energy demands**

533 Total energy use in buildings is determined by a combination of thermal demands and
534 occupier electrical loads. Thermal demands for space heating and cooling depend upon
535 local climatic conditions, building envelope thermal insulation, solar shading, and
536 occupancy rates, but tend to be proportional to total envelope area (façades plus roof,
537 through which heat losses and gains occur). Occupier electrical loads and domestic hot
538 water demands depend upon user needs and occupancy rates but tend to be
539 proportional to floor area (Bellusi et al., 2019). For any PV/T system to be useful, there
540 must be a demand for both electricity and low-grade heat, and the solar collectors
541 must be coupled to the building's heating and electrical systems (Affolter et al., 2006;
542 Zondag, 2008; Calise et al., 2016).

543 Demands for electricity are often reasonably well matched to the diurnal and seasonal
544 availability of solar resources, especially in hot and sunny climates where summertime
545 cooling demands are significant (Sorgato et al., 2018). Even when supply and demand
546 are ill-matched, excess electricity can often be utilised effectively by exporting it to the
547 mains electricity grid or storing it in batteries (Kats and Seal, 2012). Domestic hot
548 water demand is typically reasonably constant throughout the year and can be an
549 effective way of utilising the heat produced by PV/T systems provided that the heat
550 can be delivered at a sufficiently high temperature (with consequent sacrifice of PV
551 efficiency, as demonstrated by Figure 16) and stored in sufficient quantity without
552 significant heat losses. Whilst the required temperatures can be readily achieved in
553 warm and sunny climates, it is more difficult in cold and windy climates, and the
554 provision of heat loss control features (such as single or double transparent covers)
555 reduces PV efficiency and also increases the risk of stagnation overheating when hot
556 water demands are low. Space heating is typically the largest thermal demand for
557 buildings in cool climates and can be accomplished using relatively low heat delivery

558 temperatures in many cases (eg underfloor heating) but unfortunately, the greatest
559 need (during winter) does not occur when the best solar resource is available (during
560 summer). This issue is clearly problematic for latitude tilted and near-horizontal (eg
561 roof mounted) collectors which typically receive 2 to 5 times more insolation in summer
562 than they do in winter (refer to Table 1 in our study introduction paper, Part 1 of 2).
563 The seasonal solar resource variance is however much less pronounced in the case of
564 facade integrated collectors. Seasonal mismatches between solar resource availability
565 and heat demands can, in principle, be dealt with by using thermal storage but the
566 vessels required tend to be prohibitively large and supply temperatures limited (too
567 low for domestic hot water or conventional hydronic heating systems employing
568 radiators). These issues are often cited as major barriers against the widespread
569 adoption of PV/T and other types of solar space heating.

570 **4.2 Heat pump integration**

571 More than a decade ago, Zondag (2008) suggested that: "*More experience should be*
572 *obtained for unglazed PV/T collectors combined with a heat pump, since this may be a*
573 *promising development for the future*". Subsequent research investigating the use of
574 low temperature heat from PV/T systems as a thermal source for heat pumps appears
575 to have been somewhat scarce (Good et al., 2015; Qu et al., 2016; Calise et al., 2016)
576 until very recently (Lazzarin et al., 2019; Shao et al., 2020; Yao et al., 2020; Zhou et
577 al., 2020). Stagnation overheating during times of low thermal demand and transient
578 overheating disrupting compressor start-up are common themes in these recent
579 studies. Overheating in PV/T heat pump systems not only reduces PV electrical
580 efficiency and increases risk of damage to collectors (especially those featuring
581 transparent covers and air gaps to reduce heat losses) but also poses problems for
582 heat pump operation (eg excessive refrigerant pressures which impair compressor
583 function and damage seals etc). As demonstrated in our study introduction paper (Part
584 1 of 2) the BIPV-PLVTD-ICSSWH concept provides a passive means of preventing
585 overheating and stabilising temperature fluctuations, thus representing a promising
586 avenue for further development.

587 **4.3 Façade integration**

588 The BIPV-PLVTD-ICSSWH concept is intended to be integrated into building facades
589 and is particularly relevant for multi-storey buildings where the roof area is small
590 compared to the total façade area and the usable floor area. Whilst vertical façade-
591 mounted solar collectors generally receive lower levels of irradiance than tilted roof-
592 mounted collectors, and are more likely to be subjected to shading from surrounding

593 buildings and trees, the total solar resource incident on multi-storey building facades
594 is commonly greater than that incident on the roof owing to the much larger overall
595 area. In new buildings and major refurbishments, façade mounted solar collectors
596 should ideally be an integral part of the façade design and construction process (rather
597 than a bolt-on addition) for reasons of aesthetics, economics and maintainability.
598 Façade integration of a BIPV-PLVTD-ICSSWH involves a variety of design drivers and
599 constraints, some of which are common to conventional BIPV installations, and others
600 which primarily relate to the ICSSWH element. These include:

- 601 • **Visual appearance** is recognized as a crucial consideration for (and potential
602 barrier against) widespread adoption of BIPV and BISTS. Absorber surface colours
603 and planar forms can be manipulated to achieve architectural expression or
604 alternatively to “camouflage” collectors if preferred (Tripanagnostopoulos et al.,
605 2000; Affolter et al., 2006; and COST, 2015). The absorber surface and any
606 transparent covers need to be aesthetically appropriate and their dimensions
607 need to be compatible with the building facade’s structural grid.
- 608 • **Relatively high capital costs** of BISTS are often seen as prohibitive. However,
609 collector components (such as insulation, exterior weather facing surface,
610 structure) can replace elements of the façade resulting in net cost reductions
611 compared to bolt-on solutions. Collectors also produce energy which means that
612 the façade will partially or wholly “pay for itself” over time.
- 613 • **Façade zone and structural compatibility** constraints may limit overall BIPV-
614 PLVTD-ICSSWH depth or limit tank volumes. The form of the device inherently
615 needs to be slender in order to fit within the depth of conventional façade
616 constructions. The weight of the stored water in the tank will impose significant
617 structural loads on façade structural elements and/or floor slab edges in addition
618 to self-weight and wind loads, hence a compromise between desired storage
619 capacity and structural loading constraints must be sought. Fixings and pipe
620 penetrations must not compromise the integrity of the structure and should
621 ideally be readily accessible for inspections and maintenance.
- 622 • **Electrical compatibility** with conventional cabling and inverter arrangements
623 is important to ensure interoperability with existing market solutions. PV panel
624 voltages and shading tolerance needs to be considered. Micro-inverters may be
625 a good solution in these respects. Cable routes should be accessible and avoid
626 clashes with structural elements.

- 627 • **Thermal compatibility** with conventional façade thermal insulation,
628 condensation control, and ventilation strategies. Integrated BIPV-PLVTD-
629 ICSSWH collectors must not significantly add to building heat loads when the
630 stored water is hot (eg during summer). Likewise, the collectors and associated
631 pipework must not compromise the envelope by causing thermal bridging or
632 creating condensation problems.
- 633 • **Protection of PV cells** against mechanical and thermal stress, weathering and
634 humidity, as well as electrical isolation from the collector main body (metal).
635 The issue of thermal stress should not be underestimated, especially given the
636 problems encountered with temperature induced PV cell cracking observed
637 during the experiments undertaken in the present study.
- 638 • **Robustness and stability** of construction materials and joints/interfaces with
639 due regard to operating and stagnation temperatures; thermal expansion
640 stresses; exposure to precipitation (rain, snow, hail, and atmospheric moisture);
641 wind loads, and UV radiation. The water storage tank must withstand the self-
642 weight of the water it contains (together with any applied water pressure) and
643 the PLVTD must maintain a reliable vacuum, thus these components require
644 dimensional stability to ensure negligible leak risk.
- 645 • **Maintenance** of collector components needs careful consideration. Components
646 requiring regular maintenance should be accessible from inside the building.
647 Where this proves impossible, the cost and complexity of access to façade
648 mounted collectors on tall building can be minimized by utilizing available façade
649 access equipment (window cleaning cradles etc) and ensuring that façade access
650 strategies consider collector maintenance.
- 651 • **Other façade design requirements** such as fire protection, fire safety of
652 component materials, and sound insulation may also be relevant factors in the
653 design of a viable BIPV-PLVTD-ICSSWH system.

654 The abovementioned opportunities and constraints were considered insofar as possible
655 during the design of the prototype examined in this study, but further work will be
656 required to refine the concept through consultation with architects, façade engineers
657 and other construction professionals. Issues concerning costs, structural loading and
658 material robustness are the main areas of design risk to be addressed in future studies.

659 One of the most unique aspects of the BIPV-PLVTD-ICSSWH concept is the thermal
660 diode component. Whilst our experimental prototype functioned adequately during the

661 laboratory tests, the pumped evaporator wetter mechanism was found to be
662 problematic in respect of vacuum leakage, excessive power consumption, and uneven
663 wetting of the evaporator plate which impaired the forward mode thermal diode
664 performance (described in more detail by Pugsley et al., 2017 & 2020). It was also
665 found that the strut array support structure inside the PLVTD (see Figure 4) was
666 difficult to fabricate. Further development of the PLVTD component will focus on the
667 use of passive evaporator wetting mechanisms (such as capillary wicking) and trialling
668 alternative structural support arrangements.

669 **5 Conclusions**

670 This two-part study examined an alternative space-and-energy-efficient approach to
671 BIPV/T which combines BIPV, ICSSWH, and PLVTD concepts. Our first paper (Part 1 of
672 2) established the novelty and rationale for the concept and used theoretical modelling
673 to predict behaviour. The present paper (Part 2 of 2) described the realisation of a
674 prototype; presented results of multi-day solar simulator laboratory tests to validate
675 the theoretical model; identified key practical considerations and areas for future
676 design improvement; and discussed the key benefits and challenges associated with
677 integrating BIPV-PLVTD-ICSSWH concepts into NZEB facades as part of global
678 decarbonisation efforts to tackle the climate crisis.

679 The vertically oriented BIPV-PLVTD-ICSSWH prototype ($A_1=1\text{m}^2$ absorber & PLVTD
680 area with 75% PV cell coverage; $x=70\text{mm}$ PLVTD depths; $u=0.1\text{m}^3$ hot water store)
681 was tested using a solar simulator under representative scenarios (6h exposure at
682 $G=370, 610$ and 870 W/m^2 with and without transparent cover followed by 18h
683 darkness, repeated for 4 daily cycles) to examine multi-day behaviour. Measurements
684 quantified time variant absorber ($19<T_1<89^\circ\text{C}$) and stored water ($17<T_3<61^\circ\text{C}$)
685 temperatures; instantaneous solar thermal ($26<\eta_T<68\%$) and photovoltaic
686 ($5.6<\eta_E<11.8\%$) collection efficiencies; whole-module temperature dependent
687 current-voltage characteristics ($19<V_{oc}<24\text{V}$, $K_{V:T} = -0.38\%/K$, $1.5<I_{sc}<4.5\text{A}$,
688 $K_{I:T} \approx -0.04\%/K$, $66<FF<81\%$); heat loss coefficients ($21<U_{r,\text{sys}}A_{\text{sys}}/u<29\text{W}\cdot\text{m}^{-3}\text{K}^{-1}$);
689 and diurnal thermal efficiencies ($24<\eta_{T,24}<46\%$). Key findings were as follows:

- 690 • From a common starting condition of $T_3 \approx T_a \approx 17^\circ\text{C}$, water storage tank
691 temperatures were observed to reach Day 4 maxima of $T_3 = 61, 53, 40$ and
692 57°C respectively for $G=870, 610$ and 370 W/m^2 irradiance tests without
693 transparent cover and $G=610\text{ W/m}^2$ irradiance tests with transparent cover.
- 694 • Solar thermal efficiencies with and without the transparent cover were found to
695 be $\eta_{T,\text{col}}=60\%$ and 58% respectively under zero heat loss conditions

696 (N=0.0 m²K·W⁻¹), falling to $\eta_{T,col}$ =49% and 40% respectively at the benchmark
697 solar thermal condition (N=0.035 m²K·W⁻¹).

698 • Measured overnight heat loss coefficients were $U_{r,sys}A_{sys}/u = 23.0$ and
699 25.4 W·m⁻³K⁻¹ respectively with and without the transparent cover,
700 corresponding to 18h heat retention efficiencies of $\eta_{T,ret}$ 71% and 69%.

701 • Compared to modelled values, measured water storage tank temperatures were
702 typically within $\pm 3^{\circ}\text{C}$, solar thermal collection efficiencies were typically within
703 $\pm 3\%$, and specific overnight heat loss coefficients were typically within
704 $\pm 3 \text{ W}\cdot\text{m}^{-3}\text{K}^{-1}$, indicating that the theoretical model is suitably valid to enable
705 thermal performance predictions across diurnal and seasonal timescales.

706 • Overall maximum power point PV module efficiencies were observed to reduce
707 with increasing absorber temperature from $\eta_{E,mp}$ = 11.4% (at $T_1 \approx 25^{\circ}\text{C}$) to
708 5.6% (at $T_1 \approx 89^{\circ}\text{C}$) without transparent cover. Adding the transparent cover
709 reduced performance to $\eta_{E,mp} = 9.8\%$ (at $T_1 \approx 25^{\circ}\text{C}$). Allowing for issues
710 associated with PV cell cracks and transparent cover delamination, the
711 measured trends in PV performance were broadly as expected, indicating that
712 the core elements of the theoretical model are valid.

713 Whilst the experimental prototype functioned adequately during the laboratory tests,
714 opportunities for design refinements have been identified to support realisation of pre-
715 commercial prototypes focussed on integration into conventional architectural facades
716 and building services systems, including:

717 • Use of passive evaporator wetting mechanisms and alternative internal
718 structural support arrangements within the PLVTD.

719 • Optimisation of integrated thermal storage sizing to accommodate diurnal and
720 seasonal supply and demand mismatches; provide stable temperatures to
721 support operation as a thermal source for heat pumps; minimise potential for
722 stagnation overheating during hot and sunny low heat demand periods; and
723 satisfy structural loading constraints associated with weight of storage media.

724 The BIPV-PLVTD-ICSSWH façade concept provides a passive means of addressing
725 overheating and thus represents a promising avenue for further development. Issues
726 concerning costs, structural loading and material robustness do however need to be
727 addressed as part of a multi-disciplinary design approach to support realisation of
728 NZEBs as part of global efforts to tackle the climate crisis.

729 **Acknowledgements**

730 This research was enabled in its early stages by studentship funding support from the
731 Northern Ireland Department for the Economy. The work was subsequently progressed
732 with funding support from SolaForm Ltd and was completed as part of the
733 "SolaNetwork" project funded by the UKRI Engineering and Physical Sciences Research
734 Council (EP/T004819/1). The authors would also like to thank networking support
735 funded by the European Union FP7 COST Action TU1205 "Building Integration of Solar
736 Thermal Systems".

737

738 **Nomenclature**

739 ***Latin symbols***

740	A	Surface area [m ²]
741	c _p	Specific heat capacity at constant pressure [J·kg ⁻¹ K ⁻¹]
742	FF	Photovoltaic Fill Factor [%]
743	G	Solar irradiance [W·m ⁻²]
744	H	Solar insolation [MJ·m ⁻²]
745	I	Electrical current [A]
746	K	Photovoltaic performance correction coefficients [% or %/K]
747	M	Mass [kg]
748	N	Solar Thermal Condition [m ² ·K·W ⁻¹]
749	q	Thermal or electrical power [W]
750	R	Thermal or electrical resistance [K·W ⁻¹]
751	t	Time [s]
752	T	Temperature [°C]
753	$\bar{T}_{[t]}$	Average temperature, during time period [°C]
754	u	Volume [m ³]
755	U	Thermal conductance or heat transfer coefficient [W·m ⁻² K ⁻¹]
756	V	Electrical voltage [V]
757	x	Distance along an axis which is parallel to the PLVTD depth [m]
758	y	Distance along horizontal axis perpendicular to PLVTD depth [m]
759	z	Distance along an axis which is perpendicular to x and y axes [m]
760		

761 ***Greek and other symbols***

762	α	Absorptivity
763	ΔT	Temperature difference [°C]
764	η	Efficiency [%]
765	τ	Transmissivity
766		

767 ***Subscripts***

768	0	Photovoltaic cells
769	1	Planar Liquid-Vapour Thermal Diode, Plate 1 which is the evaporator in forward mode

770	2	Planar Liquid-Vapour Thermal Diode, Plate 2 which is the condenser on forward mode
771	3	Hot water storage tank
772	4	Sidewalls of the Planar Liquid-Vapour Thermal Diode
773	5	External surface of the solar absorber
774	6	Transparent element covering solar absorber
775	0a	Between PV cells and ambient environment
776	03	Between PV cells and hot water storage tank
777	1a	Between solar absorber and ambient environment
778	12	Between (or average of) the two plates
779	15	Between the PLVTD and the external surface of the solar absorber (through the laminate)
780	24	Diurnal period of 24 hours
781	3a	Between water storage tank and ambient environment
782	3ia	Between water storage tank and ambient environment through insulation
783	4ia	Between insulated PLVTD sidewalls and ambient environment
784	56	Across the air gap between the solar absorber and transparent cover
785	a	Ambient environment
786	col	Collection (period of solar absorber illumination, eg daytime)
787	E	Electrical
788	f	Forward mode
789	load	Connected electrical load
790	mpp	Maximum Power Point
791	oc	Open circuit
792	P	Pump
793	PV	Photovoltaic
794	r	Reverse mode
795	ret	Retention (period without solar absorber illumination, eg night-time)
796	sc	Short circuit
797	STC	At Standard Test Conditions
798	sys	Whole system
799	T	Thermal
800	I:T	Current-Temperature relationship
801	V:T	Voltage-Temperature relationship
802	V:G	Voltage-Irradiance relationship
803		

804 **Abbreviations**

805	AM	Air Mass index
806	BIPV	Building Integrated PhotoVoltaics
807	BISTS	Building Integrated Solar Thermal Systems
808	ICSSWH	Integrated Collector-Storage Solar Water Heater
809	mc-si	Mono-crystalline silicon
810	NZEB	Net Zero Energy Building
811	nZEB	Nearly Zero Energy Building
812	PLVTD	Planar Liquid-Vapour Thermal Diode
813	PV/T	Photovoltaic-Thermal
814	STC	Standard Test Conditions (for PV cells and modules)

815 **References**

- 816 Affolter, P., Eisenmann, W., Fechner, H., Rommel, M., Schaap, A., Soerensen, H., Tripanagnostopoulos, Y. Zondag, H. (2006). PVT
817 Roadmap – European guide for the development and market introduction of PV-Thermal technology. Petten, Netherlands: Energy
818 research Centre of the Netherlands (ECN). Available at: <<http://www.pvtforum.org/pvtroadmap.pdf>> [Last Accessed 10 January 2014]
- 819 Arya, F., Moss, R., Hyde, T., Shire, S., Henshall, P., Eames, P. (2018). Vacuum enclosures for solar thermal panels Part 2: Transient
820 testing with an uncooled absorber plate. *Solar Energy* 174, 1224-1236
- 821 Belussi, L., Barozzi, B., Bellazzi, A., Danza, L., Devitofrancesco, A., Fanciulli, C., Ghellere, M., Guazzi, G., Meroni, I., Salamone, F.,
822 Scamoni, F., Scrosati, C. (2019). A review of performance of zero energy buildings and energy efficiency solutions. *Journal of Building*
823 *Engineering* 25 (2019) 100772
- 824 Bosch (2010). High performance – Stable yields. Bosch Solar Cell M 2BB. [Last accessed: 10 September 2016]. Arnstadt, Germany:
825 Bosch Solar Energy AG. Available at: <<http://www.bosch-solarenergy.com>>.
- 826 Calise, F., d'Accadia, M, Figaj, R., Vanoli, L., (2016). A novel solar-assisted heat pump driven by photovoltaic/thermal collectors:
827 Dynamic simulation and thermoeconomic optimization. *Energy* 95, 346-66
- 828 COST Action TU1205 (2015). Overview of BISTS state of the art, models and applications. ISBN: 978-9963-697-16-8. Cyprus
829 University of Technology / European Union Horizon 2020.
- 830 Drosou, V., Tsekouras, P., Oikonomou, T., Kosmopoulos, P., Karytsas, C. (2014). The HIGH-COMBI project: High solar fraction
831 heating and cooling systems with combination of innovative components and methods. *Renewable and Sustainable Energy Reviews*
832 29 (2014) 463–472
- 833 Dupeyrat, P., Menezo, C., Rommel, M., Henning, H. (2011). Efficient single glazed flat plate photovoltaic-thermal hybrid collector for
834 domestic hot water systems. *Solar Energy* 85, 1457-68
- 835 Fayaz, H., Rahim, N., Hasanuzzaman, M., Nasrin, R., Rivai, A. (2019) Numerical and experimental investigation of the effect of
836 operating conditions on performance of PVT and PVT-PCM. *Renewable Energy* 143 (2019) 827-841
- 837 Good, C., Andresen, I., Hestnes, A. (2015). Solar energy for net zero energy buildings – A comparison between solar thermal, PV
838 and photovoltaic-thermal (PV/T) systems. *Solar Energy* 122, 986–96
- 839 Hasanuzzaman, M., Malek, A., Islam, M., Pandey, A., Rahim, N. (2016). Global advancement of cooling technologies for PV systems:
840 A review. *Solar Energy* 137 (2016) 25-45
- 841 Kats, G., Seal, A. (2012). Buildings as Batteries: The Rise of 'Virtual Storage'. *The Electricity Journal* 25 (10) 59-70
842 <http://dx.doi.org/10.1016/j.tej.2012.11.004>
- 843 Kazemian, A., Hosseinzadeh, M., Sardarabadi, M., Passandideh-Fard, M. (2018). Experimental study of using both ethylene glycol and
844 phase change material as coolant in photovoltaic thermal systems (PVT) from energy, exergy and entropy generation viewpoints. *Energy*
845 162 (2018) 210-223
- 846 Krauter, S. (2004). Development of an integrated solar home system. *Solar Energy Materials & Solar Cells* 82 (2004) 119–130
- 847 Lazzarin, R., Noro, M. (2019). Photovoltaic/Thermal (PV/T) / ground dual source heat pump: optimum energy and economic sizing
848 based on performance analysis. *Energy and Building AIP* (<https://doi.org/10.1016/j.enbuild.2020.109800>)
- 849 Muhumuza, R., Zacharopoulos, A., Mondol, J., Smyth, M., Pugsley, A., Giuzio, G., Kurmis, D. (2019). Experimental investigation of
850 horizontally operating thermal diode solar water heaters with differing absorber materials under simulated conditions. *Renewable*
851 *Energy*, Volume 138, August 2019, Pages 1051-1064
- 852 NASA - National Aeronautics and Space Administration (2019). Data Access Viewer for Prediction of Worldwide Energy Resource
853 (POWER) Project funded through the NASA Earth Science/Applied Science Program. Hampton, USA: Langley Research Center
854 (LaRC). Available at: < <https://power.larc.nasa.gov/data-access-viewer/> > [Last accessed: 07/10/19].
- 855 Pugsley, A., Mondol, J., Smyth, M., Zacharopoulos, A., Di Mattia, L. (2016). Experimental characterisation of a flat panel integrated
856 collector-storage solar water heater featuring a photovoltaic absorber and a planar liquid-vapour thermal diode. *Proceedings of 11th*
857 *ISES EuroSun Conference: Palma (Mallorca), Spain from 11 to 14 October 2016*. Martinez, V. & Gonzalez, J. (eds.).
- 858 Pugsley, A. (2017). Theoretical and experimental analysis of a novel flat photovoltaic-thermal solar water heater with integrated
859 energy storage via a planar liquid-vapour thermal diode. Ulster University PhD Thesis (uk.bl.ethos.713462) published July 2017.

- 860 Pugsley, A., Zacharopoulos, A., Mondol, J., Smyth, M. (2019). Theoretical and experimental analysis of a horizontal Planar Liquid-
861 Vapour Thermal Diode (PLVTD). *International Journal of Heat and Mass Transfer* 144 (2019) 11866
- 862 Pugsley, A., Zacharopoulos, A., Mondol, J., Smyth, M. (2020). Vertical Planar Liquid-Vapour Thermal Diodes (PLVTD) and their
863 application in building façade energy systems. *Applied Thermal Engineering* (submitted for publication 01/2020, under review)
- 864 Qu, M., Chen, J., Nie, L., Li, F., Yu, Q., Wang, T. (2016). Experimental study on the operating characteristics of a novel
865 photovoltaic/thermal integrated dual-source heat pump water heating system. *Applied Thermal Engineering* 94, 819–26
- 866 Shao, N., Ma, L., Zhang, J. (2020). Experimental investigation on the performance of direct-expansion roof-PV/T heat pump system.
867 *Energy* 195 (2020) 116959
- 868 Smyth, M., Eames, P. Norton, B. (2003). Heat Retaining Integrated Collector/Storage Solar Water Heaters. *Solar Energy* 75, 27-34
- 869 Smyth, M., Besheer, A., Zacharopoulos, A., Mondol, J., Pugsley, A., Novaes, M. (2015). Experimental evaluation of a Hybrid
870 Photovoltaic/Solar Thermal (HyPV/T) Façade Module. *Proceedings EURO ELECS Conference 21-23 July 2015, Guimarães, Portugal.*
- 871 Smyth, M., Quinlan, P., Mondol, J., Zacharopoulos, A., McLarnon, D., Pugsley, A. (2018). The experimental evaluation and improvements
872 of a novel thermal diode pre-heat solar water heater under simulated solar conditions. *Renewable Energy* 121, 116-122
- 873 Smyth, M., Pugsley, A., Hanna, G., Zacharopoulos, A., Besheer, A., Savvides, A. (2019). Experimental performance characterisation
874 of a Hybrid Photovoltaic/Solar Thermal Façade module compared to a flat Integrated Collector Storage Solar Water Heater module.
875 *Renewable Energy* 137 (2019) 137-143
- 876 Sorgato, M., Schneider, K., Rüter, R. (2018). Technical and economic evaluation of thin-film CdTe building-integrated photovoltaics
877 (BIPV) replacing façade and rooftop materials in office buildings in a warm and sunny climate. *Renewable Energy* 118 (2018) 84-98
- 878 Stackhouse, P., Zhang, T., Westberg, D., Barnett, A., Bristow, T., Macpherson, B., Hoell, J. (2018). POWER Release 8.0.1 (with GIS
879 Applications) Methodology, Data Parameters, Sources, & Validation. Data Version 8.0.1. Web Site Version 1.1.0. Hampton, USA:
880 NASA LaRC, Langley Research Center.
- 881 Tripanagnostopoulos, Y., Souliotis M. and Nousia, T. (2000). Solar Collectors with Coloured Absorbers. *Solar Energy* 68 (4) 343-356
- 882 Yang, T., Athienitis, A. (2016). A review of research and developments of building-integrated photovoltaic/thermal (BIPV/T) systems.
883 *Renewable and Sustainable Energy Reviews* 66 (2016) 886–912
- 884 Yao, J., Xu, H., Dai, Y., Huang, M. (2020). Performance analysis of solar assisted heat pump coupled with build-in PCM heat storage
885 based on PV/T panel. *Solar Energy* 197 (2020) 279–291
- 886 Zacharopoulos, A., Mondol, J., Smyth, M., Hyde, T., O'Brien, V. (2009). State of the Art Solar Simulator with Flexible Mounting.
887 *Proceedings ISES Solar World Congress, 11-14 October 2009, Johannesburg, South Africa, pp 854-863*
- 888 Zhou, J., Zhu, Z., Zhao, X., Yuan, Y., Myers, S. (2020). Theoretical and experimental study of a novel solar indirect expansion heat
889 pump system employing mini channel PV/T and thermal panels. *Renewable Energy AIP* (doi.org/10.1016/j.renene.2019.11.054)
- 890 Ziapour, B., Palideh, V., Mohammadnia, A. (2014). Study of an improved integrated collector-storage solar water heater combined
891 with the photovoltaic cells. *Energy Conversion and Management* 86 (2014) 587–594.
- 892 Zondag, H. (2008). Flat-plate PV–thermal collectors and systems: a review. *Renewable & Sustainable Energy Reviews* 12, 891–959.